DESIGN AND ANALYSIS OF DUAL SHAPE CORE FIBER BASED REFRACTIVE INDEX SENSOR

A Dissertation submitted towards the partial fulfillment of the requirement for the award of degree of

Master of Technology
in
Microwave and Optical Communication

Submitted by

Pradeep Kumar Tewari

2K11/MOC/08

Under the supervision of

Dr. Ajeet Kumar
(Assistant Professor)

DEPARTMENT OF
ELECTRONICS AND COMMUNICATION ENGINEERING
&
APPLIED PHYSICS
DELHI TECHNOLOGICAL UNIVERSITY, DELHI
(FORMERLY DELHI COLLEGE OF ENGINEERING)

JUNE 2013

CERTIFICATE

This is to certify that the dissertation title ***"Design and Analysis of Dual Shape Core Fiber Based Refractive Index Sensor"*** is the authentic work of **Mr. Pradeep Kumar Tewari** under my guidance and supervision in the partial fulfillment of requirement towards the degree of Master of Technology in ***Microwave and Optical Communication***, jointly run by the Deptt. of Electronics & Communication Engineering and Deptt. of Applied Physics in ***Delhi Technological University, Delhi.***

Dr. Ajeet Kumar	Prof. S.C. Sharma	Prof. Rajiv Kapoor
Supervisor	Head of Deptt.	Head of Deptt.
Assistant Professor	Deptt. of Applied Physics	Deptt. of ECE
Delhi Technological University	Delhi Technological University	Delhi Technological University

ACKNOWLEDGEMENT

I am indebted to my thesis supervisor **Dr. Ajeet Kumar**, Assistant Professor, for his gracious encouragement and very valued constructive criticism that has motivated me to carry the project successfully.

I am deeply grateful to **Prof. Rajiv Kapoor**, Head of Department of Electronics and Communication Engineering, Delhi Technological University for his support and encouragement in carrying out this project.

I wish to express my heart full thanks to **Prof. S.C. Sharma**, Head of Department of Applied Physics and my branch coordinators **Prof. R.K Sinha & Dr. Priyanka Jain,** Assistant Professor, for their support that helped me a lot in successful completion of this project.

I express my deep sense of gratitude to **Mr. Gautam Prabhakar** & **Mr. Akhit Peer** for their time to time supports and encouragements.

Finally I would like to thank to the *Holy Almighty* "*OM*" for his blessings without which nothing is possible in this world.

Pradeep Kumar Tewari

M.Tech (MOC)

2K11/MOC/08

Table of Contents

List of Figures

ABSTRACT

A sensor (also called detector) is a converter that measures a physical quantity and converts it into a signal which can be read by an observer or by an (today mostly electronic) instrument. A sensor is a device which receives and responds to a signal when touched. A sensor's sensitivity indicates how much the sensor's output changes when the measured quantity changes. The resolution of a sensor is the smallest change it can detect in the quantity that it is measuring. Different chemical substances as well as several physical and biological parameters can be detected through measurements of the refractive index (RI). For this reason, RI sensors have gained considerable attention by the sensor community. Fiber-based refractometric devices are attractive; owing to the inherent advantages over their counterparts based on other techniques i.e. they can be multiplexed on a single fiber network and are suitable for *in situ* and remote RI measurements. Moreover, they are compact and lightweight. The resolution of fiber-based RI sensors can be as high as 10^{-5}. So far, different alternatives have been proposed to design RI sensors with conventional optical fibers. These include core-exposed or tapered fibers, fiber Bragg gratings (FBGs), long period gratings (LPGs), interferometers made with FBGs or LPGs, refractive index sensors based on core diameter mismatch etc. Technological progress allows more and more sensors to be manufactured on a microscopic scale as micro sensors using dual shape core fiber based refractive index properties.

Chapter 1

Introduction

1.1 Optical Fiber

An optical fiber is a flexible, transparent fiber made of glass (silica) or plastic, thicker up to 125-175μm. It can function as a waveguide, or "light pipe" to transmit light between the two ends of the fiber. Optical fibers are widely used in fiber-optic communications, which permits transmission over longer distances and at higher bandwidths (data rates) than other forms of communication. Fibers are used instead of metal wires because signals travel along them with less loss and are also immune to electromagnetic interference. Fibers are also used for illumination, and are wrapped in bundles so that they may be used to carry images, thus allowing viewing in confined spaces. Specially designed fibers are used for a variety of other applications, including sensors and fiber lasers.

Optical fibers typically include a transparent core surrounded by a transparent cladding material with a lower index of refraction. Light is kept in the core by total internal reflection (TIR). This causes the fiber to act as a waveguide. Fibers that support many propagation paths or transverse modes are called multi-mode fibers (MMF), while those that only support a single mode are called single-mode fibers (SMF). Multi-mode fibers generally have a wider core diameter, and are used for short-distance communication links and for applications where high power must be transmitted. Single-mode fibers are used for most communication links for long haul communications [1-5].

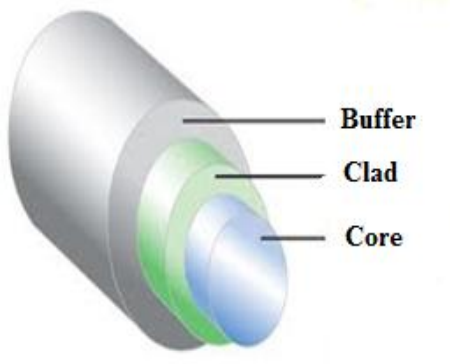

Fig. 1.1 *Schematic of a simple optical fiber*

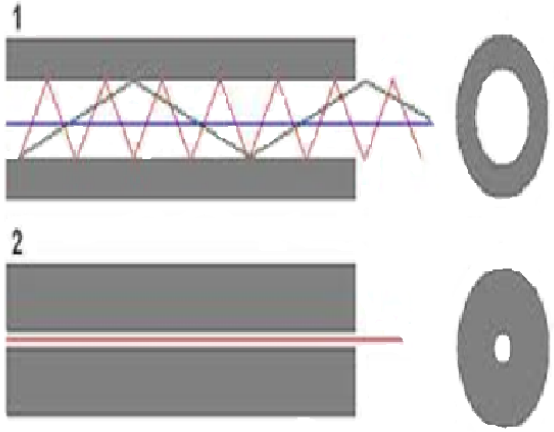

Fig. 1.2 *Schematic of a MMF & SM fibers*

1.2 Fiber-Optic Communication

In Fiber-optic communication, information is transmitted from one place to another by sending pulses of light through an optical fiber. The light forms an electromagnetic carrier wave that is modulated to carry information. Fiber-optic communication systems have given a great leap to the telecommunications industry and have played a major role in the advent of the information age. Because of its advantages over electrical transmission, optical fibers have largely replaced copper wire communications in core networks in the world. The process of communicating using fiber-optics involves the following basic steps: creating the optical signal involving the use of a transmitter, relaying the signal along the fiber, ensuring that the signal does not become too distorted or weak, receiving the optical signal, and converting it back into an electrical signal.

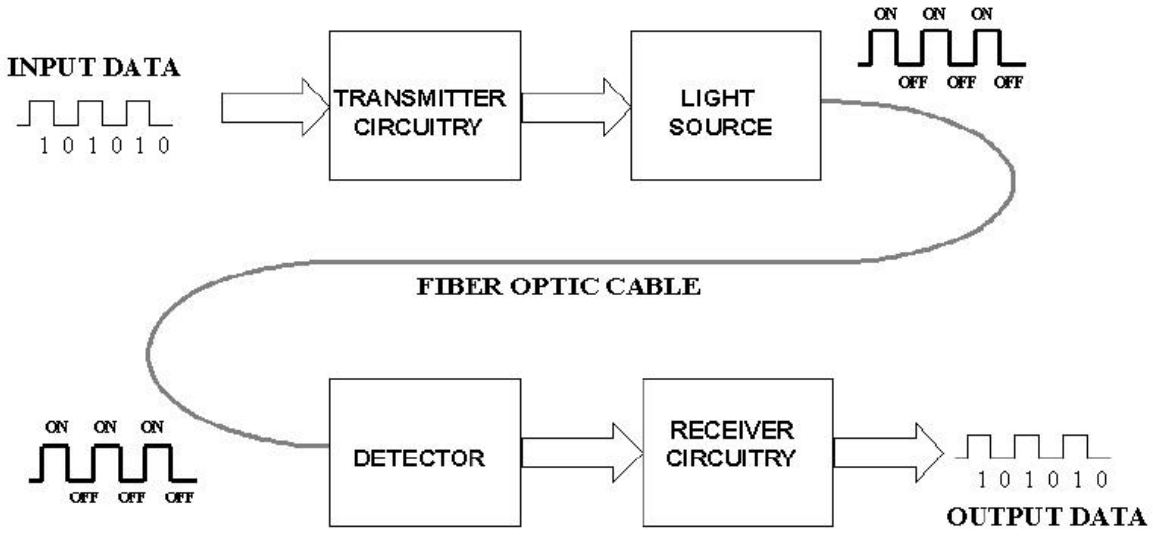

Fig 1.3 Simple optical fiber communication system

1.3 Additional Applications of Optical Fiber

Fibers are widely used in illumination applications. They are used as light guides in medical and other applications where bright light needs to be shone on a target without a clear line-of-sight path. In some buildings, optical fibers route sunlight from the roof to other parts of the building (non-imaging optics). Optical fiber illumination is also used for decorative applications, including signs, art, toys and artificial Christmas trees. Optical fiber is also used in imaging optics. A coherent bundle of fibers is used, sometimes along with lenses, for a long, thin imaging device called an endoscope, which is used to view objects through a small hole. Medical endoscopes are used for minimally invasive exploratory or surgical procedures in spectroscopy, optical fiber bundles transmit

light from a spectrometer to a substance that cannot be placed inside the spectrometer itself, in order to analyze its composition. A spectrometer analyzes substances by bouncing light off and through them. By using fibers, a spectrometer can be used to study objects remotely. An optical fiber doped with certain rare earth elements such as erbium can be used as the gain medium of a laser or optical amplifier. Optical fibers doped with a wavelength shifter collect scintillation light in physics experiments. Optical fiber can be used to supply a low level of power (around one watt) to electronics situated in a difficult electrical environment. Examples of this are electronics in high-powered antenna elements and measurement devices used in high voltage transmission equipment. A fiber optic sensor is a sensor that uses optical fiber either as the sensing element ("intrinsic sensors"), or as a means of relaying signals from a remote sensor to the electronics that process the signals ("extrinsic sensors"). Fibers have many uses in remote sensing. Depending on the application, fiber may be used because of its small size, or because no electrical power is needed at the remote location, or because many sensors can be multiplexed along the length of a fiber by using different wavelengths of light for each sensor, or by sensing the time delay as light passes along the fiber through each sensor. Intelligent transportation systems, such as smart highways with intelligent traffic lights, automated tollbooths, and changeable message signs, also use fiber-optic-based telemetry systems. Another important application for optical fiber is the biomedical industry. Fiber-optic systems are used in most modern telemedicine devices for transmission of digital diagnostic images. Other applications for optical fiber include space, military, automotive, and the industrial sector [6-8].

1.4 Refractive Index Sensor

Different chemical substances as well as several physical and biological parameters can be detected through measurements of the refractive index (RI). For this reason, RI sensors have gained considerable attention by the sensor community. Fiber-based refractometric devices are attractive, owing to the inherent advantages over their counterparts based on other techniques. For example, they can be multiplexed on a single fiber network and are suitable for *in situ* and remote RI measurements. Moreover, they are compact and lightweight. In addition, the amount of sample needed to carry out the measurements can be very small. The resolution of fiber-based RI sensors can be as high as 10^{-5}. So far, different alternatives have been proposed to design RI sensors with conventional optical fibers. These include core-exposed or tapered fibers, fiber Bragg gratings (FBGs), long period gratings (LPGs) interferometers made with FBGs or LPGs, refractive index sensors based on core diameter mismatch etc. The advent of micro-structured optical fibers has also opened new possibilities for RI sensing [9-10].

1.5 Objectives and Organization of the Thesis

This thesis is concerned with the design and analysis of dual shape core optical fiber based refractive index sensor, with a core diameter mismatch which is very much a topical area of research. Prior to this a single mode core diameter mismatch refractive index sensor has been developed in which the sensing region has been achieved by etching out the whole cladding and some portion of the core of the fiber. If the sensing region surrounded by different external medium the power transfer from the input end to output end varies. This fractional power transfer gives us the refractive index of the medium. So the objective of this thesis is to design and analysis of dual shape core fiber based refractive index sensor by core diameter mismatch.

The thesis consists of six chapters. Each chapter has its own introduction. This dissertation has been ordered in such a way that the process of constructing the proposed design and analysis of dual shape core fiber based refractive index sensor is evident throughout. Proceeding in a logical manner.

Chapter 2 introduces the specialty fibers.

Chapter 3 focus is placed on refractive index based optical fiber sensors.

Chapter 4 focus is placed on the method of analysis which includes transfer matrix method and transfer of power method which is a powerful tool for the analysis of refractive index sensors.

Chapter 5 presents the design and analysis of proposed novel design for refractive index sensing.

Chapter 6 finally, the conclusion and scope for the future work are given in this chapter.

Chapter 2

Classification of Optical Fiber

Optical fiber can be used as a medium for telecommunication and computer networking because it is flexible and support wide bandwidth. It is especially advantageous for long-distance communications, because light propagates through the fiber with little attenuation compared to copper cables. This allows long distances to be spanned with few repeaters. Additionally, the per-channel light signals propagating in the fiber have been modulated at rates as high as 111 gigabits per second by NTT [11, 12], although 10 or 40 Gbit/s is typical in deployed systems [13, 14]. Each fiber can carry many independent channels, each using a different wavelength of light (wavelength-division multiplexing (WDM)). The net data rate (data rate without overhead bytes) per fiber is the per-channel data rate reduced by the forward error correction (FEC) overhead, multiplied by the number of channels (usually up to eighty in commercial dense WDM systems as of 2008). The transmission efficiency increases using dense wavelength-division multiplexing (DWDM) by reducing the spacing between the channels. As of 2011 the record for bandwidth on a single core was 101 Tbit/sec (370 channels at 273 Gbit/sec each). The record for a multi-core fibre as of January 2013 was 1.05 peta bits per second. In 2009, Bell Labs broke the 100 (Petabit per second)×kilometre barrier (15.5 Tbit/s over a single 7000 km fiber) [15-17].

For short distance application, such as a network in an office building, fiber-optic cabling can save space in cable ducts. This is because a single fiber can carry much more data than electrical cables such as standard category-5 Ethernet cabling, which typically runs at 100 Mbit/s or 1 Gbit/s speeds. Fiber is also immune to electrical interference; there is no cross-talk between signals in different cables, and no pickup of environmental noise. Non-armored fiber cables do not conduct electricity, which makes fiber a good solution for protecting communications equipment in high voltage environments, such as power generation facilities, or metal communication structures prone to lightning strikes. They can also be used in environments where explosive fumes are present, without danger of ignition. Wiretapping (in this case, fiber tapping) is more difficult compared to electrical connections, and there are concentric dual core fibers that are said to be tap-proof [18].

Fibers have many uses in remote sensing. In some applications, the sensor is itself an optical fiber. In other cases, fiber is used to connect a non-fiber optic sensor to a measurement system. Depending on the application, fiber may be used because of its small size, or the fact that no electrical power is needed at the remote location, or because many sensors can be multiplexed along the length of a fiber

by using different wavelengths of light for each sensor, or by sensing the time delay as light passes along the fiber through each sensor. Time delay can be determined using a device such as an *optical time-domain reflectometer* (OTDR). Optical fibers can be used as sensors to measure strain, temperature, pressure and other quantities by modifying a fiber so that the property to measure modulates the intensity, phase, polarization, wavelength, or transit time of light in the fiber. Sensors that vary the intensity of light are the simplest, since only a simple source and detector are required. A particularly useful feature of such fiber optic sensors is that they can, if required, provide distributed sensing over distances of up to one meter.

Extrinsic fiber optic sensors use an optical fiber cable, normally a multi-mode one, to transmit modulated light from either a non-fiber optical sensor or an electronic sensor connected to an optical transmitter. A major benefit of extrinsic sensors is their ability to reach otherwise inaccessible places. An example is the measurement of temperature inside aircraft jet engines by using a fiber to transmit radiation into a radiation pyrometer outside the engine. Extrinsic sensors can be used in the same way to measure the internal temperature of electrical transformers, where the extreme electromagnetic fields present make other measurement techniques impossible.

Extrinsic sensors measure vibration, rotation, displacement, velocity, acceleration, torque, and twisting. A solid state version of the gyroscope, using the interference of light, has been developed. The *fiber optic gyroscope* (*FOG*) has no moving parts, and exploits the *Sagnac effect* to detect mechanical rotation. Common uses for fiber optic sensors include advanced intrusion detection security systems. The light is transmitted along a fiber optic sensor cable placed on a fence, pipeline, or communication cabling, and the returned signal is monitored and analysed for disturbances. This return signal is digitally processed to detect disturbances and trip an alarm if an intrusion has occurred. In addition to applications in optical communications, specialty fibers find a wide range of applications in other fields, such as biomedical power delivery and imaging systems, military fiber gyroscope, and high power lasers. A few such fibers are described in the following:

2.1 Bragg Fiber

A fiber Bragg gratings (FBGs) is a type of distributed Bragg reflector constructed in a short segment of optical fiber that reflects specific wavelengths of light and transmits all others. This is achieved by creating a periodic variation in the refractive index of the fiber core, which generates a wavelength specific dielectric mirror. A fiber Bragg grating can therefore be used as an inline optical filter to block certain wavelengths, or wavelength-specific reflector. The primary application of fiber Bragg gratings is in optical communication system used as notch filters. They are also used in optical multiplexers and de-multiplexers with an optical circulator or optical add-drop multiplexer (OADM).

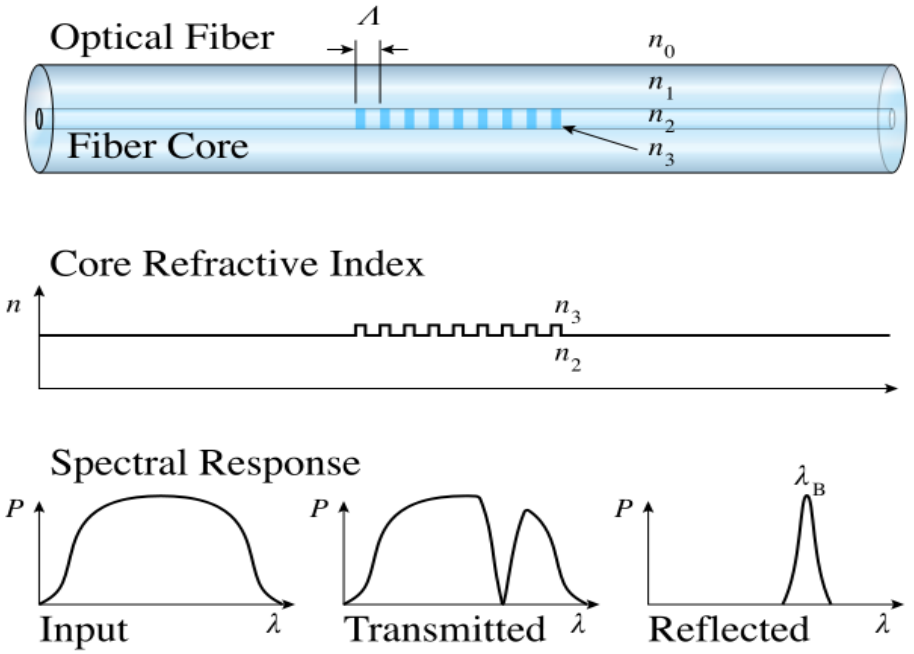

Fig 2.1 A FBG structure, with refractive index profile and spectral response

Figure 2.2 shows 4 channels optical circulator. The FBG is set to reflect one of the channels, here channel 4. The signal is reflected back to the circulator where it is directed down and dropped out of the system. Since the channel has been dropped, another signal on that channel can be added at the same point in the network. A de-multiplexer can be achieved by cascading multiple drop sections of the OADM, where each drop element uses an FBG set to the wavelength to be de-multiplexed. Conversely, a multiplexer can be achieved by cascading multiple add sections of the OADM. FBG de-multiplexers and OADMs can also be tunable. In a tunable de-multiplexer or OADM, the Bragg wavelength of the FBG can be tuned by strain applied by a piezoelectric transducer.

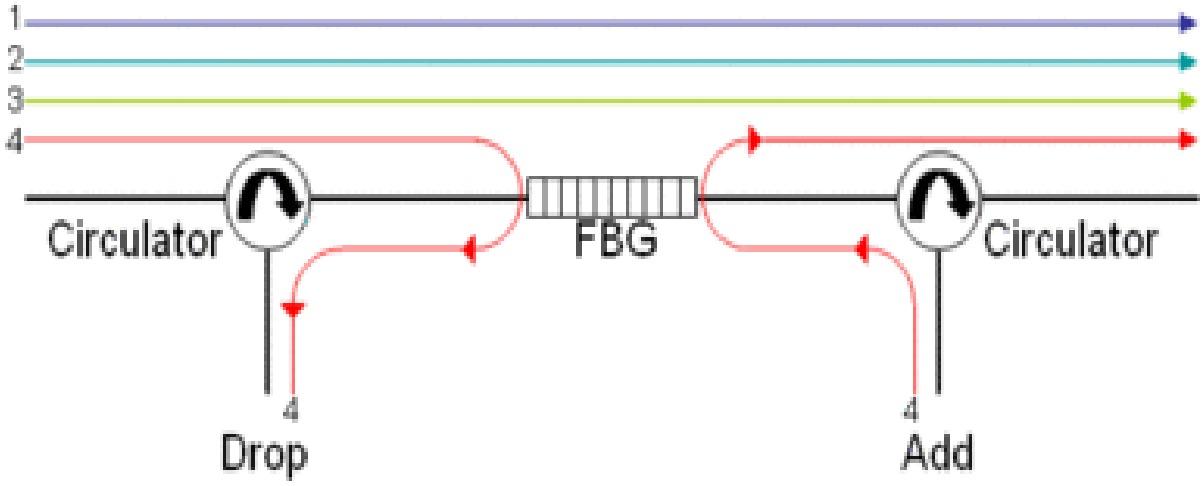

Fig 2.2 Optical add-drop multiplexer

The Bragg wavelength is also sensitive to temperature. Using this property the fiber Bragg gratings can be used as sensing elements in optical fiber sensors. In a FBG sensor, the measure and causes a shift in the Bragg wavelength, $\Delta\lambda_B$.

2.2 Photonic Crystal Fiber

Photonic-crystal fiber (PCF) also known as holey fiber is a new class of optical fiber based on the properties of photonic crystals. Because of its ability to confine light in hollow cores or with confinement characteristics not possible in conventional optical fiber, PCF is now finding applications in fiber-optic communications as well as endlessly single-mode fiber, fiber lasers, nonlinear devices, high-power transmission, highly sensitive gas sensors, and other areas. More specific categories of PCF include photonic-band gap fiber (PCFs that confine light by band gap effects), holey fiber (PCFs using air holes in their cross-sections), hole-assisted fiber (PCFs guiding light by a conventional higher-index core modified by the presence of air holes), and Bragg fiber (photonic-band gap fiber formed by concentric rings of multilayer film). Photonic crystal fibers may be considered a subgroup of a more general class of micro-structured optical fibers, where light is guided by structural modifications, and not only by refractive index differences. Photonic crystal fibers can be divided into two modes of operation, according to their mechanism for confinement. Those with a solid core, or a core with a higher average index than the micro-structured cladding, can operate on the same index-guiding principle as conventional optical fiber, however, they can have a much higher effective- refractive index contrast between core and cladding, and therefore can have much stronger confinement for applications in nonlinear optical devices, polarization-maintaining fibers, (or they can also be made with much lower effective index contrast). Alternatively, one can create a "photonic band gap" fiber, in which the light is confined by a photonic band gap created by the micro-structured cladding such a band gap, properly designed, can confine light in a lower-index core and even a hollow (air) core.

Band gap fibers with hollow cores can potentially circumvent limits imposed by available materials, for example to create fibers that guide light in wavelengths for which transparent materials are not available (because the light is primarily in the air, not in the solid materials). Another potential advantage of a hollow core is that one can dynamically introduce materials into the core, such as a gas that is to be analyzed for the presence of some substance. PCF can also be modified by coating the holes with sol-gels of similar or different index material to enhance its transmittance of light.

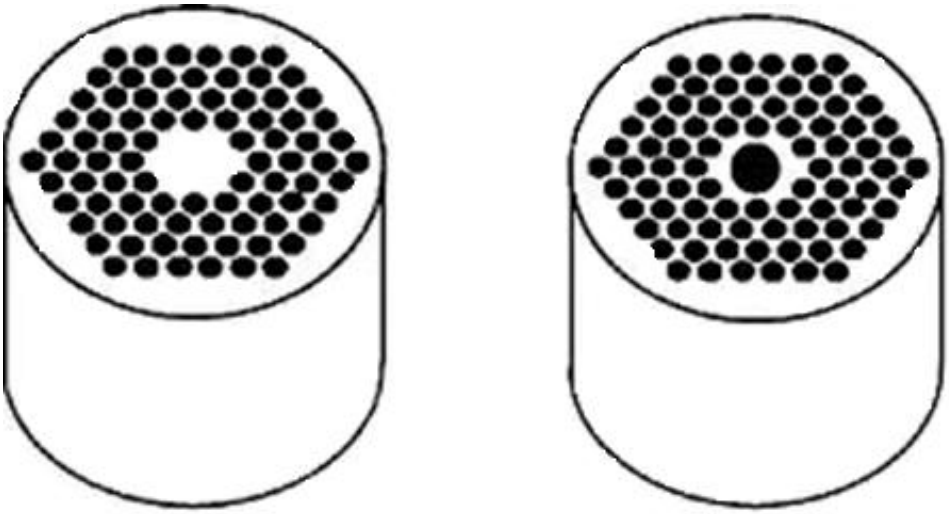

Note: Black circles indicate Air Holes in silica (White) background

Fig 2.3 Photonic crystal fibre, solid core and air core structures

2.3 Segmented Cladding Fiber

Another type of fiber, known as Segmented cladding fiber (SCF) were proposed as an alternative to the holey fibers of single mode operation over an extended range of wavelengths. It was then shown that an SCF could be designed as an ultra large core single mode fiber for optical communication, which could suppress effectively the non-linear optical effects because of its large core size. It also provides a much higher transmission capacity because of its potentially weak birefringence, compared with a holey fiber [19]

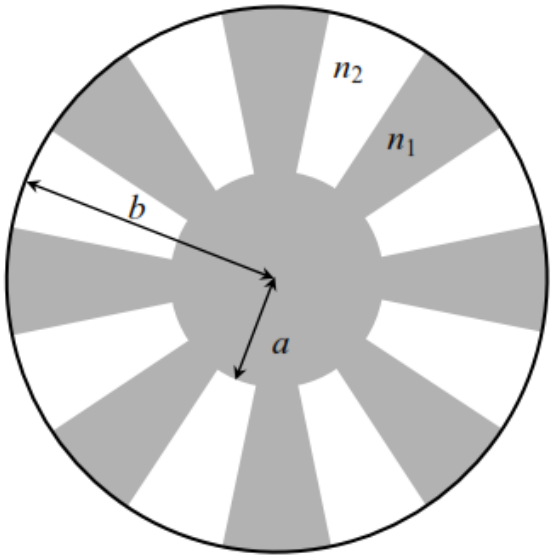

Fig. 2.4 Structure of a segmented cladding fiber

A SCF is characterized by the cladding with regions of high and low refractive index alternating regularly with uniform core of high refractive index. The SCF uses small index contrast unlike holey fiber and hence exhibits some better qualities over photonic crystal fibers. It has potentially low polarization mode dispersion which is essential for high bit rate transmission. The chromatic dispersion of SCF is also expected to be similar to that of conventional fiber so that it can be controlled by conventional techniques. An SCF can be bare segmented cladding fiber or coated segmented cladding fiber. For the former, the segmented cladding is surrounded by air and for the later, the segmented cladding of the SCF extends to infinity. The effective index decreases monotonously towards the core index and eventually exceeds the mode index of the fundamental mode. An infinitely extended SCF is therefore a leaky structure and all the modes of the fiber suffer from leakage loss. In practice, the fiber is truncated a finite cladding radius and coated with a high index material. A high index surrounding is similar to that of an infinitely extended cladding and at the same time shields the fiber from external perturbations.

2.4 Large Mode Area Fiber

For some applications, it is desirable to use optical fibers with effective large mode areas (*LMA fibers*) often with single-mode property. Due to the reduced optical intensities, such fibers effectively have lower nonlinearities and a higher damage threshold, which makes them suitable for, e.g., the amplification of intense pulses or single-frequency signals in fiber amplifiers, or in the case of passive fibers for delivery of such light. Whereas standard single-mode fibers have an effective mode area below $100\mu m^2$, large mode area fibers reach values of hundreds or even thousands of μm^2. Note that waveguide dispersion becomes weak for large mode areas. Therefore, there is limited scope for tailoring the chromatic dispersion of large mode area fibers.

A straightforward design approach to obtain large mode areas is to decrease the numerical aperture (NA) by to decrease the refractive index difference between the core and the cladding, for a step-index fiber design. However, there are severe limitations: the guidance (wave guiding) then becomes weak, and significant losses can arise from small imperfections of the fiber or from bending losses. Therefore, the numerical aperture cannot be made smaller than approximately 0.06. To achieve relatively robust single-mode guidance at larger mode areas, there are several more refined design approaches with specially optimized refractive index profiles, which allow for mode areas up to the order of $1000\mu m^2$. This is an order of magnitude higher than for ordinary single-mode fibers. There are additional difficulties in applying this concept to rare-earth-doped fibers. Relatively high concentrations of additional dopants are often required, and these dopants often increase the numerical aperture. Even if the refractive index contrast can be reduced in some way, the precision of

refractive index control may be decreased, and this affects the ability to realize very large mode areas. Somewhat larger mode areas can be achieved with fiber designs supporting a few propagation modes (*multimode fibers*). It may then still be possible to guide light dominantly in the fundamental mode, so that the output e.g. of a fiber amplifier is close to diffraction-limited [20- 22]. Stringent limitations arise from the more critical launch conditions and from mode mixing in the fiber, which can spoil the beam quality and lead to beam pointing fluctuations [23]. Various more sophisticated fiber designs (partly based on photonic crystal fibers) and techniques have been developed for addressing these challenges. In many cases, one attempts to introduce substantial propagation losses for any higher-order modes, making it easier to maintain robust single-mode propagation in a multimode fiber. Another important aspect is to minimize unwanted mode coupling. To date, most work in this area has concentrated on rare-earth-doped optical fiber with large mode area to improve their energy storage characteristics in compromise of gain efficiency. A number of erbium doped fiber with large mode area have been fabricated which demonstrated their effectiveness as optical amplifiers and in Q-switched fiber lasers. Shizhuo et al. made a new design of fiber having large effective area over 100 μm^2 which can be used in DWDM system for its non-zero dispersion shifting characteristics. This fiber also showed low bending and splicing loss [24].

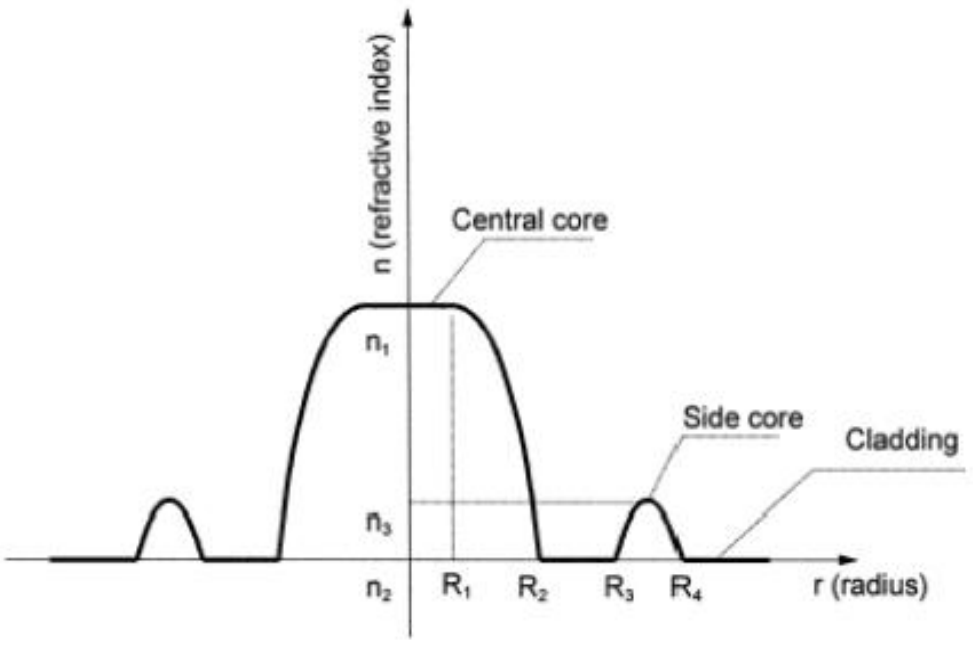

Fig. 2.5 Refractive index profile of a fiber designed by Shizhuo et al [24]

2.5 Raised Inner Cladding Fiber

Raised inner cladding fiber consists of five layers of which four layers form the cladding. The cladding layers have low and high indices alternatively.

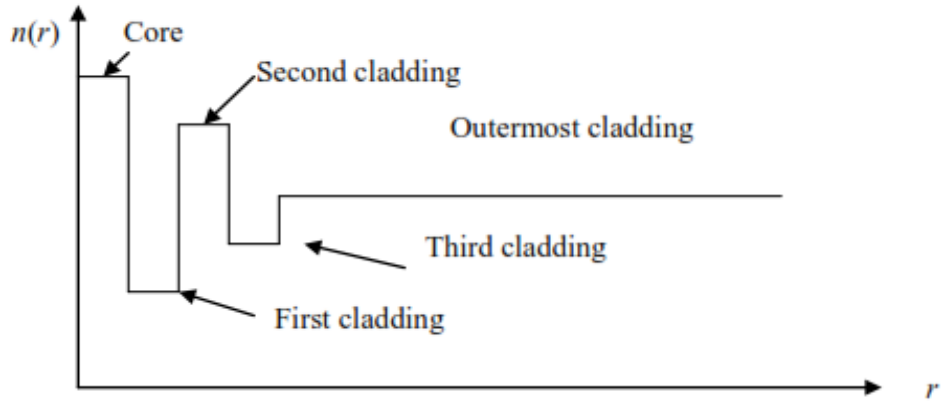

Fig.2.6 Refractive index profile of a typical raised inner cladding fiber

The objective of this structure has low loss and low dispersion at both the 1.3μm and 1.55μm wavelengths. This fiber shows uniform dispersion properties in this wavelength range.

2.6 Depressed Inner Cladding (DIC) Fiber

These fibers have two claddings and are also called double clad fibers. Each cladding has a refractive index that is lower than that of the core. Of the two claddings, inner and outer, the inner cladding has the lower refractive index. A doubly clad fiber has the advantage of very low macro bending losses. It also has two zero-dispersion points and low dispersion over a much wider wavelength range than a singly clad fiber [26].

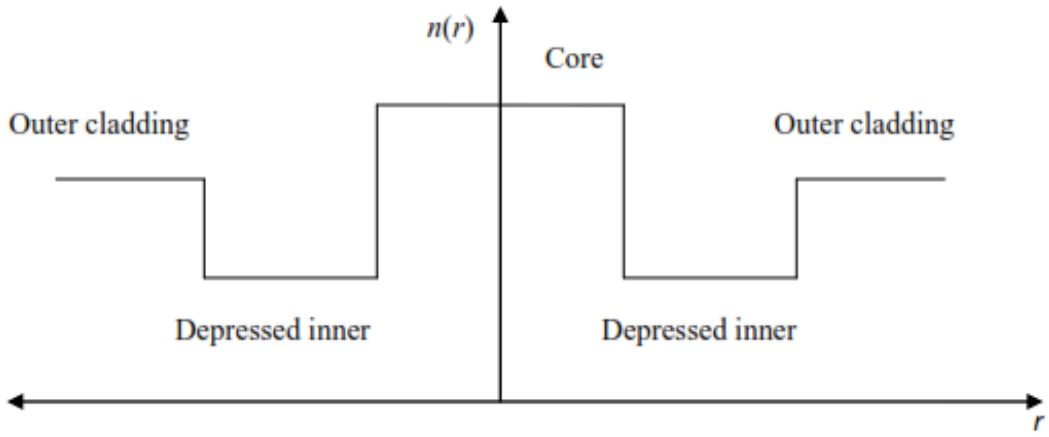

Fig 2.7 Refractive index profile of typical DIC fiber [26]

2.7 Polarization - Maintaining Optical Fibers and Their Applications to Sensing

High-birefringent polarization-maintaining fibers are studied theoretically and experimentally. Results obtained and analyzed with formulas for birefringence and modal dispersion and for high-birefringent elliptical fibers by variational method with a Gaussian approximation. Already discussed regarding birefringence, dispersion and electric field distributions of single- and double-clad elliptical fibers. Based on an analysis of the elliptical fiber, strain and temperature sensitivities without built-in stresses calculated. Different designs presented to minimize the temperature or strain sensitivities by suitably selecting the fiber parameters, such as core ellipticity, refractive index difference and thickness of the inner cladding and resulted that a double-clad elliptical fiber is more flexible for this design. A novel method for minimizing the temperature sensitivity of PM fiber with high strain sensitivity is proposed using a double-clad elliptical fiber with stress applying inner elliptical cladding. This is achieved by suitably selecting doping materials for the core and the inner cladding to balance the built-in stresses in the core and cladding of the fibers and the temperature and strain sensitivities and the design of temperature-insensitive fibers with high strain sensitivities are suitable for polarimetric strain sensors.

An example of the fiber design is given and the strain sensitivity of 50 rad/mm is obtained with zero temperature sensitivity. A dynamic polarimetric fiber-optic measuring system built. The strain and temperature sensitivities of three common types of high-birefringent PM fibers: bow-tie, PANDA and elliptical core fibers are measured. The measurement process is automatic and controlled by a microprocessor or PC. The results match well with other publications. Polarization properties of high-birefringent elliptical fibers under bending and lateral pressure are studied using coupled-mode theory. Bending and pressure effects are treated as perturbations to refractive index by photo elastic theory. Numerical results given in terms of various fiber parameters, the normalized frequency, the ratio of the major axis to the minor axis of the core, the ratio of the inner cladding major axis to the core major axis, and the difference between the core index and the inner cladding index. For the special case of a circular single -mode fiber, the results agree with the existing publications. Finally, some potential applications of temperature -insensitive PM fibers in polarimetric sensing systems discussed. Smart structures and skins, electric and magnetic field sensors, current, acoustic, displacement, acceleration and flow rate sensors among the possibilities. Finally suggested a future research for two-mode highly elliptical fibers [27].

Chapter 3

Refractive Index Based Optical Fiber Sensors

Out of many novel working mechanism of fiber optics sensor types which have been discovered, the following ones have often being used:

1) Fiber Bragg gratings (FBGs), which couple the forward propagating core mode to the backward propagating core mode.
2) Long-period fiber gratings (LPFGs), which couple the forward propagating core mode to one, or a few, of the forward propagating cladding modes.
3) Fabry-Perot (FP) fiber sensors, which use the Fiber optics in an interferometric setting for sensing very small mechanical deformations.
4) Core diameter mismatches sensors, which makes the device sensitive to the external refractive index.

3.1 Leaky Cladding Mode Propagation in Long - Period Fiber Grating Devices

Fiber gratings are passive waveguide structures that permit control over the wavelength, polarization, direction, and modal characteristics of light in an optical fiber. In particular, long-period fiber gratings are transmissive devices that couple co-propagating modes of the fiber. In a single-mode fiber (SMF), the ability to couple to cladding modes provides for several useful device applications such as loss filtering. The spectral characteristics of these filters are generally constant, but it is conceivable to actively tailor the filter spectrum if, for example, the cladding of the long-period grating were jacketed in an optically active material. Unfortunately, the refractive index of most amenable materials exceeds that of the cladding, thus precluding total internal reflection (TIR), and therefore true guided-wave propagation. However, if the refractive index of the material surrounding the cladding is sufficiently greater than that of the cladding, mere Fresnel reflection could enable reasonably low-loss propagation for device applications.

Coupling to leaky modes in along-period fiber grating experiment, several long-period gratings were fabricated in hydrogen-loaded Corning Flex core fiber and then submerged into various refractive index oils in order to quantify the phenomenon. Coupling to the $HE_{1,6}$ cladding mode in a long-period grating with a length of 1.3cm and a period of 290μm. For $n_{Sur} > n_{c1}$ the coupling resonance shifts to shorter wavelengths as n_{Sur} increases. Once n_{Sur} exceeds n_{c1}, the resonance corresponds to leaky mode coupling and the peak transmission loss increases as n_{Sur} increases, a trend that agrees with

theoretical predictions. For the case of n_{Sur}= 1.734, the core mode transmission loss reaches -13dB, implying that about 95% of the core mode is coupled to a leaky cladding mode. These observations were compared to the results of a model in which the transmission characteristics of a long-period grating are calculated using a transfer-matrix technique. The leaky waveguide situation was simulated by introducing loss in to the cladding mode in the model. The cladding mode losses that best reproduced the experimentally observed leaky mode coupling resonances were calculated [28].

3.2 Sensitivity Characteristics of Long-Period Fiber Gratings

Various LPFGs devices have been demonstrated for use as band rejection filters, erbium-doped fiber amplifier (EDFA) gain equalizers, comb filters, mode converters, and sensors for physical parameters such as temperature, strain, refractive index (RI), and curvature. In all fields of potential application, knowledge of the sensitivity of the LPFG to the parameters of its physical environment is clearly important. For most telecommunications applications, low sensitivity is generally desirable to minimize the influence of environmental variations on device performance. For sensors, on the other hand, and for some dynamically controlled devices, high sensitivity is usually advantageous. Thus, whether it is with the objective of maximizing or of minimizing its value, full characterization of the sensitivity of the LPFG is an important precursor to practical device design. Although there have been several studies of this subject, most of them have been focused on the resonant coupling of lower order cladding modes. Recently, it is found that the higher order mode resonances exhibit some quite different and potentially advantageous properties, including a dual resonance feature that may be exploited to realize highly sensitive devices.

The central portion from 14^0C~ 24 ^{0}C, shows a near-linear response with the transmission changing from 83.6% to 16.9% across this range; the average sensitivity is -6.67% per ^{0}C, and a detector resolving 0.01% of the transmitted intensity can register a 0.002^0C temperature change. To the measurement of strain the m= 11 mode of a 203μm period LPFG. For an applied strain varied from 0με to 3000με, increasing strain decreases the coupling strength without detectable change in peak wavelength, and the near-linear transmitted intensity response yields an averaged sensitivity of 0.025% [29-32].

3.3 Non - uniform Thinned Fiber Bragg Gratings for Simultaneous Refractive Index and Temperature Measurements

Today, the necessity to monitor industrial processes, environmental or structural health, where a large number of physical or chemical features have to be measured, requires the availability of advanced sensing systems able to provide multi-functional multi parameter operation. In particular in chemical sensing applications, temperature compensated fiber-optic refractometers offer a valid alternative

over spectroscopy and fluorescence-based sensors, especially when multipoint operation is required. For long-period grating (LPG)-based sensors, the thermal compensation can be easily obtained by the simultaneous measurements of the wave length shifts related to different attenuation bands. An alternative approach is provided by combining Fabry–Perot configurations with fiber Bragg grating (FBG) operation for simultaneous measurements of temperature and refractive index. Recently, thinned fiber Bragg gratings (ThFBGs) have been proposed as high sensitive refractive index sensors providing high resolution and low-cost measurements combined with easy multiplexing capability.

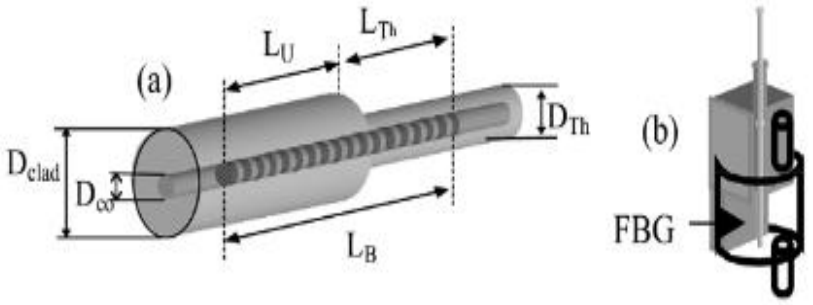

Fig.3.1 (*a*) *Schematic diagram of the structure under investigation (not in scale)* (*b*) *Experimental setup for sensor fabrication and characterization etching* (n*ot in scale*) [33]

In this case, the thermal compensation could be easily obtained by adding a standard grating element sensitive only to thermal changes. This approach, although efficient for single-point monitoring is not the suitable solution when a large number of spatial locations have to be monitored. The experimental characterization confirms the theoretical and numerical analysis carried out to predict the sensor performances. Resolutions of $\approx 10^{-5}$ and $\approx 10^{-4}$ for the SRI around 1.45 and 1.33, respectively, and resolution in temperature of 0.1^0C are possible by using easily available units [33].

3.4 High Resolution Refractive Index Sensing with Cladded Multimode Tapered Optical Fibre

In a variety of applications, the measurement of the refractive index (RI) is very important since it is a fundamental material property. In bio-sensing, for example, there is a need to measure very small RI changes in small volumes of fluid. Traditional bulk refractometers are not appropriate for such applications neither are they convenient in RI measurements where size and weight are a concern. In the above situations RI sensors based on optical fibres constitute an alternative. So far, metal-coated optical fibres, or in-fibre Bragg grating (FBG) have been proposed as highly sensitive refractometric devices. Fibre-based RI sensors can be very compact and are suitable for remote sensing. Moreover,

they can be multiplexed effectively on a single fibre network. A new fibre optic sensor suitable for the determination of the RI of non-absorbing liquids, as well as very small RI changes in the liquid. The sensor is based on the radiation losses introduced by the sample liquid in a cladded multimode tapered optical fibre (MMTF).

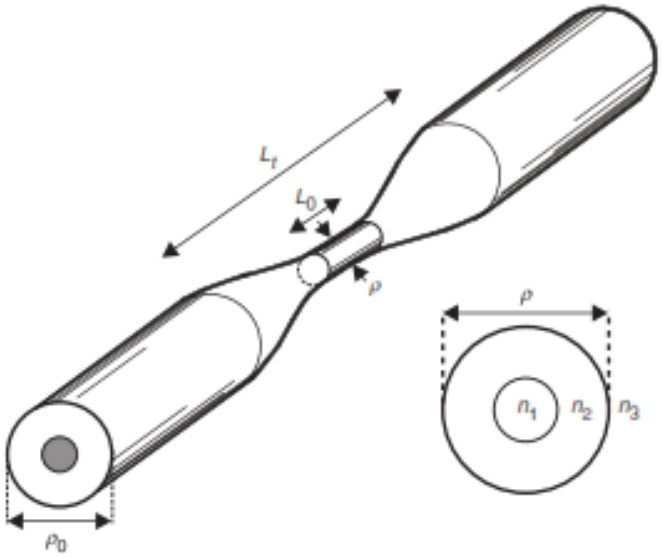

Fig. 3.2 Illustration and cross-section of cladded multimode tapered fibre [34]

The sensor sensitivity and dynamic range can be adjusted with the taper waist diameter which in turn can be easily tailored during the taper fabrication process. The sensor exhibits maximum transmission changes when the RI of the sample liquid approaches that of the fibre cladding. The low cost and the simplicity of the fibre RI sensor reported here make it attractive for some applications in which it would be necessary to sense very small RI changes in the range 1.36 to 1.46. A sensor with a large waist diameter and may offer the highest sensitivity, combined with an appropriate signal amplification, provide resolution as high as 10^{-4} [34].

3.5 Dual Core Photonic Crystal Fiber for Hydrostatic Pressure Sensing

A novel hydrostatic pressure sensor based on a dual-core photonic crystal fiber (DC-PCF). Two solid fiber cores separated by an air hole in the cross-section lead to two independent waveguides inside the DC-PCF which accompany with mode coupling. The mode coupling of two solid fiber cores of the DC-PCF under different hydrostatic pressure is numerically investigated. A pressure sensing system is proposed and performances of the pressure sensor have been numerically investigated**.** The proposed DC-PCF with a cross-section shown in Fig.3.3(a) is formed by a triangular lattice of circular air holes with two missing holes as two fiber cores (A and B) which are separated by one air hole. The hole pitch of the triangular lattice is Λ and diameter of the air hole is *d*.

Parameters of the calculated DC-PCF are Λ=2μm and d=1.4μm, respectively. Assuming refractive index of the air to be 1.0 and the refractive index of the fused silica is 1.444 at 1.55μm according to the well-known Sellmeier equation. By using commercial software based on a finite-element method (FEM) to investigate guided modes of the proposed DC-PCF. Transmission spectra of a 10cm DC-PCF for hydrostatic pressure of ranging from 0 to 1000MPa and the pressure results in the blue shift of the transmission spectrum. For peak wavelength around 1.55μm, a linear relationship between the

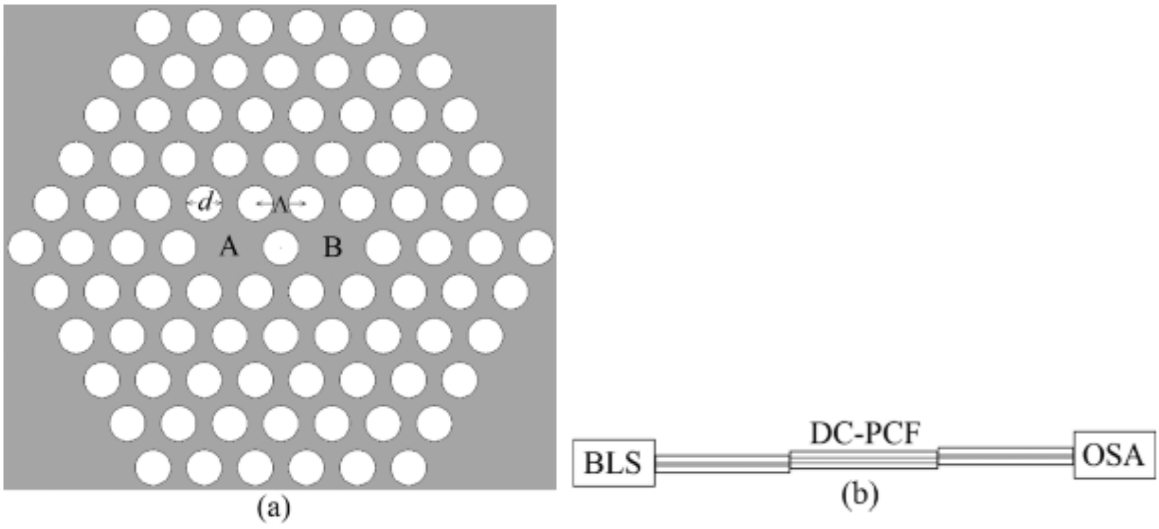

Fig. 3.3 (*a*) *Cross-section of the proposed DC-PCF,* (*b*) *Schematic diagram of a hydrostatic pressure sensing system based on the DC-PCF* [35]

peak wavelength and the pressure is observed. The sensitivity of the DC-PCF based pressure sensor is about -3.47pm/MPa. The wavelength shift response of the pressure sensor is dependent on the structure of the DC-PCF. The calculated wavelength shift of the transmission spectrum of 10-cm DC-PCFs with different structure parameters versus the pressure from 0 to 1000 MPa, the possibility to further optimize the structure of the DC-PCF for pressure sensing [35].

3.6 Refractive Index Sensing in an All-Solid Twin-Core Photonic Band Gap Fiber

A highly sensitive refractive index sensor based on a twin-core coupler in an all-solid photonic band gap guiding optical fiber. A single hole acts as a microfluidic channel for the analyte, which modifies the coupling between the cores, and avoids the need for selective filling. By operating in the band gap guiding regime the proposed sensor is capable of measuring refractive indices around that of water, and because the analyte varies the coupling coefficient the device is capable of both high sensitivity and a relatively large dynamic range. The proposed PBG MOF sensor has a single microfluidic analyte channel (refractive index n_e) between two solid and identical low index cores. The two cores

are separated by two times the pitch, i.e 2Λ and the cladding is a triangular array of high-index rods of diameter d=0.53Λ, separated by a pitch of Λ=3.2 μm.

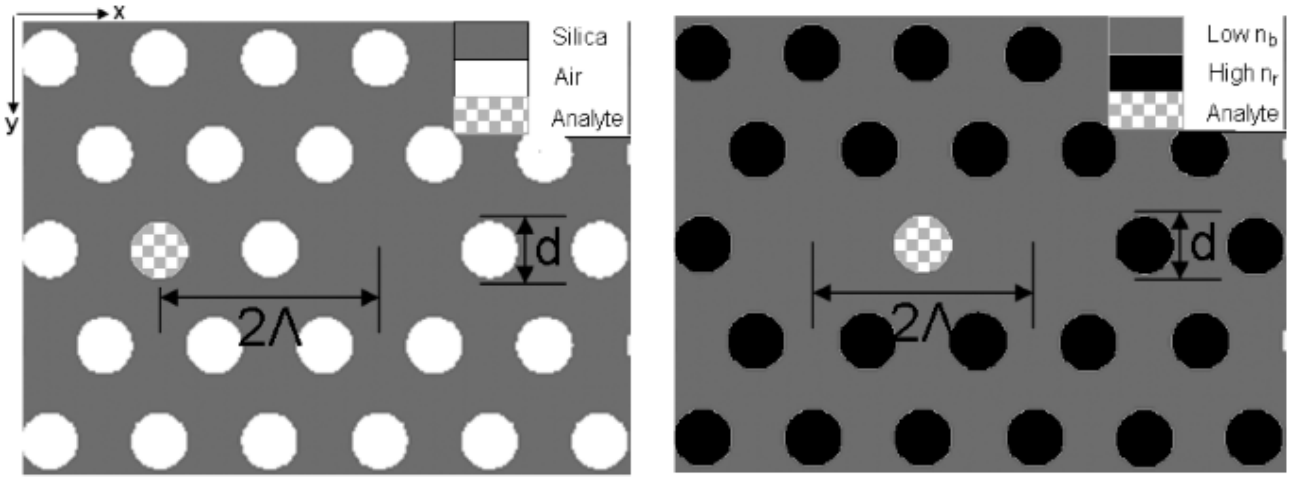

(a) (b)

Fig. 3.4 Triangular microstructure with pitch Λ and hole diameter d of
(*a*) *the twin-core index-guiding MOF and*
(*b*) *proposed solid twin core PBG sensor, fabricated from a host material with low index* n_b *and rod inclusions with higher index* n_r [36]

Here the fiber is designed to be fabricated using two different polymer materials, i.e., Poly1 and Poly2, where Poly1 is the low refractive index background material (n_b=1.34), and Poly2 is used for the high index rods (n_r=1.53). Material dispersion neglected

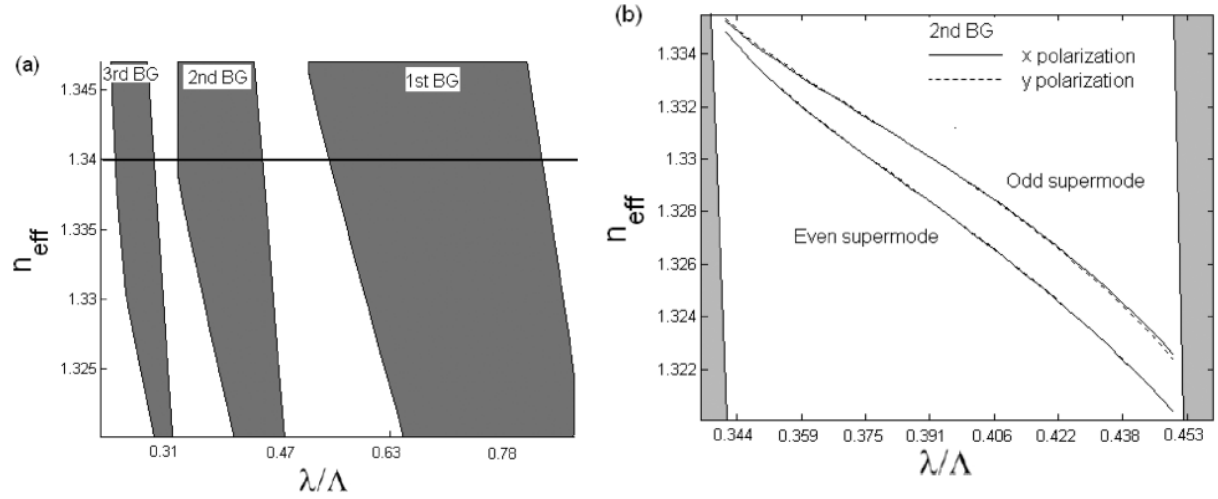

Fig. 3.5 (*a*) *PBG of one of the cores of the PGB fiber in isolation, shown as effective index* n_{eff} *versus normalized frequency λ/Λ, for* n_b*= 1.34 and* n_r*= 1.53. The refractive index of the cores is shown with a solid black line.*
(*b*) *Effective indices of the x- and y-polarized even and odd super modes in the second band gap Λ=3.2μm, d=0.53Λ* [36]

for a single wavelength. In PBG MOF, every core has broad transmission windows, or band gaps, in which optical guidance occurs. Determining the band gap wavelengths and bandwidths by the periodicity, geometry, and refractive indices of the high index inclusions relative to the low index host. The cores of the PBG MOF form a balanced directional coupler. The evanescent fields of the two cores coupled and causing a periodic transfer of optical power from one core to the other and back. The coupling can also be understood and analyzed in terms of a pair of super modes, a symmetric (even) super mode and an anti-symmetric (odd) super mode. The effective indices n_{eff} and field distributions of the even and odd supermodes of the dual-core PBG MOF were calculated using the fully vectorial finite element software COMSOL™. The effective indices in the second bandgap are shown in Fig. 3.5(b), from which we could see that the difference between the x- and y-polarized supermodes is small. Therefore we use as effective index the average effective indices of the two orthogonal polarizations, $n_{eff} = (n_x+n_y)/2$. The paper showed that the transmittance of a 1mm long sensor changed with analyte index by 65 873%/RIU and a sensor one coupling length long, in which a change in analyte refractive index by 0.001RIU led to a shift of coupling wavelength of 70nm [36].

3.7 Low Cost Optical Fiber Refractive - Index Sensor Based on Core Diameter Mismatch

The resolution of fiber-based RI sensors can be as high as 10^{-5}. So far, different alternatives have been proposed to design RI sensors with conventional optical fibers. These include core-exposed or tapered fibers, fiber Bragg gratings (FBGs), long period gratings (LPGs), interferometers made with FBGs or LPGs, etc. The advent of micro-structured optical fibers has also opened new possibilities

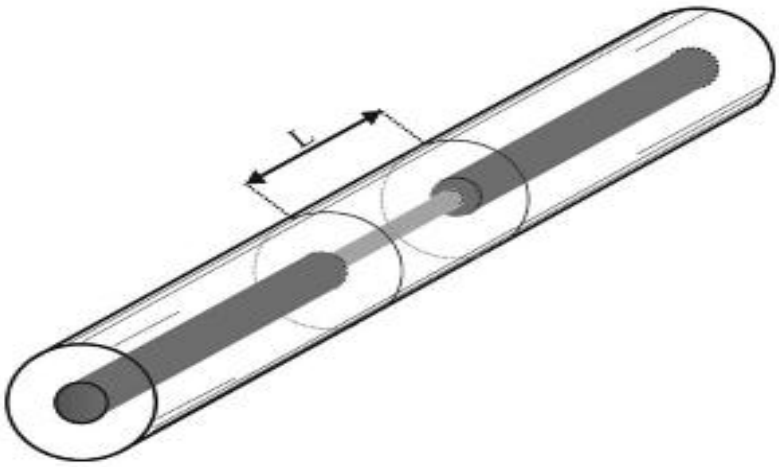

Fig.3.6 Schematic representation of the sensor. L is the section of SMF that is inserted into the multi-mode fiber. It is also the sensor interaction length [37]

for RI sensing. It should be pointed out that in the RI sensors reported, no especial coatings are needed. A core-exposed or tapered fiber can be coated with gold, so RI sensors based on the excitation of surface plasmons can be developed. The device consists of a short section of single-mode fiber (SMF), which works as a sensing element, inserted in to a multimode fiber. Owing to the core diameter mismatch, some of the light is guided by the cladding of the SMF. This makes the transmission of the device dependent on the RI of the external medium. The sensor exhibits maximum transmission changes, i.e., maximum resolution, when the index of the sample medium approaches that of the fiber cladding. Moreover standard emitters, fibers, detectors, etc., are needed to fabricate the sensor, which makes it attractive for diverse applications. Here, a new optical fiber RI sensor is presented, consisting of a short section of SMF inserted into multimode fiber. The core diameter mismatch makes the core modes of the multimode fiber couple to cladding and core modes in the SMF. The cladding modes leaked out as the RI of the medium that surrounds the SMF approaches the index of the cladding. The indexes in which the sensor exhibits maximum resolution up to 7×10^{-5} are at indexes that are closed to the index of the cladding [37].

3.8 Design and Fabrication of a Single - Mode Optical Fiber Based Refractive Index Sensor

When an optical fiber is bent and part of its cladding is stripped off, the light energy (E) emerging from the fiber depends on the refractive index of the surrounding medium (n_m). The change in n_m can be found from E. The light output energy and the measuring sensitivity are calculated numerically as a function of n_m for several values of the bending radius R. As applications of this sensor, measurement of liquid density and detection of oil are described. Here present a core diameter mismatch RI sensor designed in a single mode optical fiber. The sensing region has been achieved by etching out the whole cladding and some portion of the core of the fiber. Modulation of the modal field distribution and modulation of fractional power transfer with the RI of the external medium has been used to investigate the response of the sensor [38].

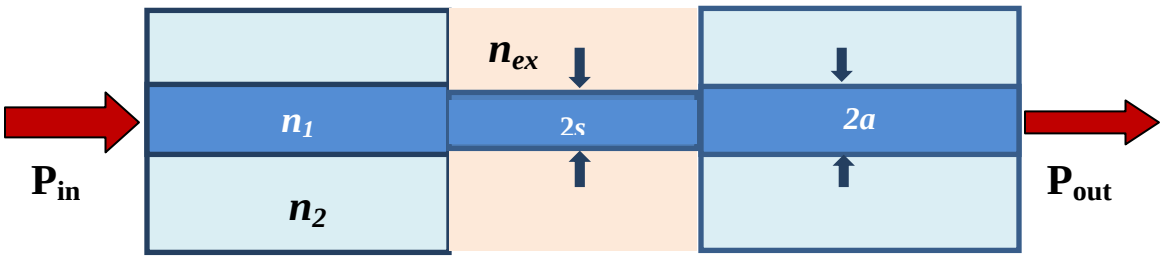

Fig. 3.7 Schematic diagram of a single-mode optical fiber based refractive-index sensor

The previous mentioned techniques having merits of single mode, single fiber and high sensitivity. Keeping core sensing region less than 3-4μm, the system become fragile for real time application. To overcome the said problem, we propose a single mode, single fiber, large mode area, core diameter mismatch and dual shape core fiber based refractive-index sensor**.**

Chapter 4

Dual Shape Core Fiber Based Refractive Index Sensor

4.1 Design and Analysis of Dual Shape Core Fiber Based Refractive Index Sensor

Fiber Optic Sensor has been of interest to researchers because of their high sensitivity and wide frequency response. The fiber optic refractive index sensor is ideal for refractive index measurement of fluids in industrial, chemical and food processing industry application. Its use allows a complete refractive analysis in the most challenging environments. Several alternatives to design refractive index sensors with conventional optical fibers and rectangular waveguides have been reported in the literature. These Long Period Gratings (LPGs), metal coated fibers using surface plasmon response, Fiber Bragg Gratings (FBGs), and tapered fibers. Recently Vilatoro and Monzon have proposed a low cost optical fiber sensor based on core diameter sensor based on core diameter mismatch obtained by splicing a short section of single mode fiber to a multimode fiber. The fiber is essentially a depressed-index clad fiber with a dual-shape-core (DSC) consisting of a large central core and a small slightly lower-index side core. The refractive indices of the two cores are so chosen as to perfectly guide the fundamental mode. All the higher-order modes of the fiber are leaky. The fiber shows large-mode-are a single-mode operation by higher-order modes discrimination. Analyzed the structure by using the transfer matrix method and Numerical simulation results suggest that the DSC fiber can have single-mode operation with effective mode area as large as 580μm^{2}and low bending loss. The bending loss of the fiber could be brought down by more than 2 orders of magnitude compared to the corresponding step-index fiber. Mode field area is relatively insensitive to design parameters in comparison to the leakage loss of the mode.

Proposed fiber consists of dual-shape-core and depressed-index leaky cladding. Refractive-index profile of the designed fiber is shown below and can be written as

$$n(r) = \begin{cases} n_1; & 0 < r < a \\ n_s; & a < r < b \\ n_2; & b < r < c \\ n_s; & r > c \end{cases} \qquad (4.1)$$

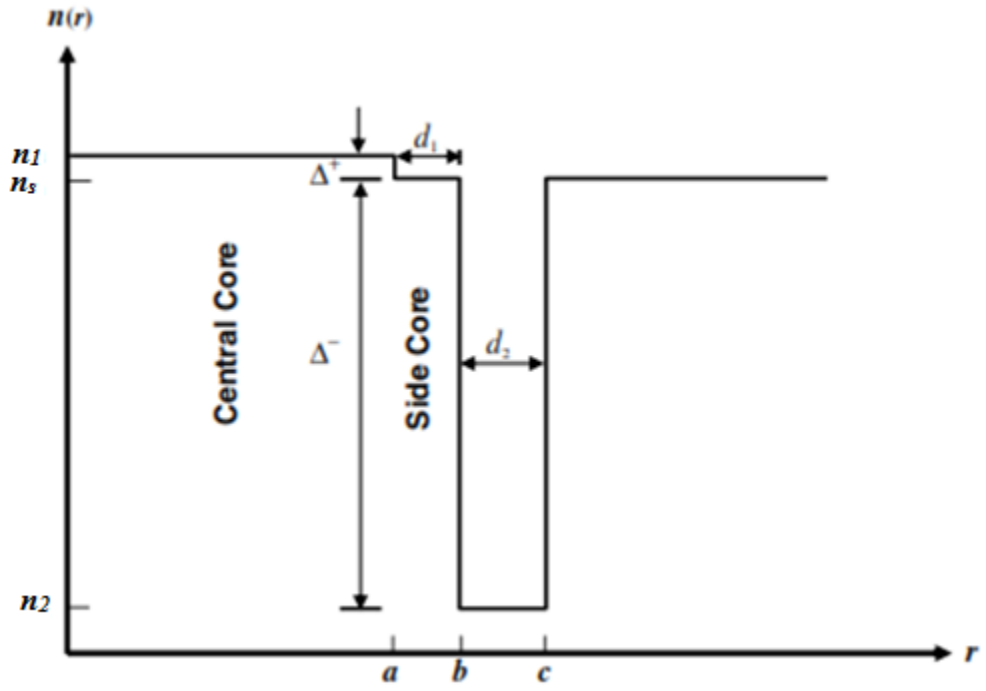

Fig.4.1 Refractive-index profile of the proposed DSC fiber

Where $n_1 > n_s > n_2$, n_s represent refractive index of silica, and Δ^+ and Δ^- represents the refractive index difference between silica and doped layers of n_1 and n_2 respectively. A high-index central core can be formed by doping germanium into silica. Δ^+ can be carefully chosen to support only a fundamental mode of the fiber for a given core radius a. A fiber with small Δ^+ can, however, is highly sensitive to bend induced loss. To overcome this problem, a trench of width d_2 and relative index difference Δ^- is introduced after distance d_1 from the central core. A low-index trench that can be formed by fluorine doping into silica is surrounded by outermost silica layer, which makes the fiber leaky only for higher-order modes. To make the discussion more comfortable widths of the various layers have been defined as $d_1 = b-a$, $d_2 = c-b$. To assess the potential of the present structure as an LMA fiber with low bend loss, investigated the bending performance of the structure with respect to d_1 and d_2. The results shows that W-fiber ($d_1 = 0$) suffers from highest bend loss for all bending radii in the range 2–20cm. Bend loss of fiber decreases with d_1 and converges at large values of d_1. Bend loss of the fiber decreases by a factor of 10 by adding aside core of width $d_1 = 4\mu m$ in W-fiber. Thus, the proposed design shows better bending performance than the large-core W-fiber. The bend loss of the fiber decreases significantly with the width of trench. Fiber with $d_2 = 0$ (conventional low NA LMA fiber) suffers from the highest bend loss among all the designs. Addition of a low-index trench of width 3μm in a conventional SM fiber at 4μm distance from the central-core reduces the bend loss from 11dB/m to 0.1 dB/m at 12cm bending radius. Thus, the proposed DSC fiber has low bend loss in comparison to corresponding W-fiber ($d_1 = 0$) and conventional large-core fiber ($d_2 = 0$) and would be

useful in applications like high power fiber lasers and amplifiers. Bending of the fiber also introduces high loss to the higher-order mode and helps in higher-order mode suppression. A fiber with such a large mode area (~580μm^2) would be useful in high power applications [40].

4.2 Transfer Matrix Method

To developing accurate numerical approximate techniques to study the propagation characteristics of absorbing, non-absorbing or leaky planar waveguide structures has been considerable interest. The use of the matrix method in studying the propagation of plane electromagnetic waves through a stratified medium is well known in optics. In essence this method involves determination of the transfer matrix of the system and then using the properties of a guided mode to obtain a characteristic equation. The solutions of this transcendental equation give the propagation constants of the modes of the waveguide. In general, the above method become tedious as the number of films increases and, in particular, become complicated for analyzing absorbing/lossy structures as they involve the solution of complex transcendental equations. The transcendental equations can be solved very easily by matrix method which is used for the analysis of the proposed structure. The present fiber is analyzed by simple method involving multiplication of 2 × 2 matrices from which we can readily obtain the real and imaginary parts of the propagation constants as well as the field configurations for arbitrarily graded planar structures. We have applied the method to obtain leakage and absorption losses in planar waveguide structure. Since exact analysis for graded index optical fibers is difficult and time-consuming, appropriate approximation techniques have been developed. Among them, scalar approximation analysis is one of the most widely used techniques.

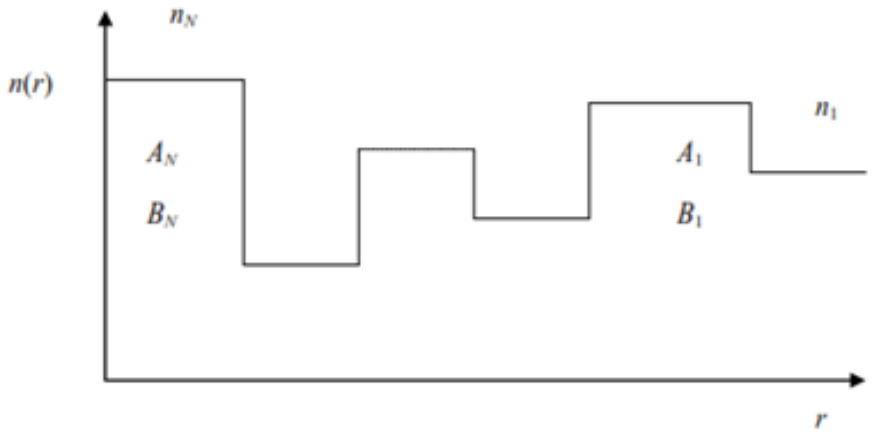

Fig.4.2 Refractive index profile of a radially symmetric optic fiber have multilayer structure

It is assumed that the permittivity of the fiber depends only on the distance *r* from the axis, and the permeability is equal to that of vacuum. We consider an optical fiber having a radially symmetric

refractive index profile and consisting of N regions having refractive indices n_1, n_2, n_3, …n_N as shown in the above Fig. Under the scalar approximation, the equation describing the radial part of the modal field in the p^{th} region is given by

$$r^2\frac{d^2R}{dr^2}+r\frac{dR}{dr}+\left[\left(k_0^2n_p^2-\beta^2\right)r^2-l^2\right]R=0 \qquad (4.2)$$

We have assumed that the modal field will be given by

$$\psi(r,\phi,z,t)=R(r)\left[\frac{\cos\phi l}{\sin\phi l}\right]\exp i(\omega t-\beta z) \qquad l=1,2,3,..... \qquad (4.3)$$

$$r^2\frac{d^2R}{dr^2}+r\frac{dR}{dr}+\left[\left(k_0^2n_p^2-\beta^2\right)r^2\right]R=0 \qquad (4.4)$$

The solution for this equation can be given analytically by standard Bessel functions which describe the transverse field inside the fiber. In the attenuating region, where $\beta^2<k_0^2n_p^2$ the general solution of equation (4.4) is given by:

$$R(r)=A_pJ_0(k_pr)+B_pY_0(k_pr) \qquad (4.5)$$

And in the Guiding region, where

$$\beta^2>k_0^2n_q^2$$

$$R(r)=A_qK_0(\gamma_qr)+B_qI_0(\gamma_qr) \qquad (4.6)$$

Where

$$k_p^2=k_0n_p^2-\beta^2;\quad \gamma_q^2=\beta^2-k_0^2n_q^2 \qquad (4.7)$$

In the scalar approximation, the boundary conditions require continuity of R and the derivative of R at each interface. In the interface of p^{th} and $(p+1)^{th}$ layer we match the boundary conditions and get a relationship between the coefficient of $(p+1)$, B_{p+1} and the coefficients of preceding layers (A_p, B_p) in a form of 2x2 matrix. The relationship is given by:

$$\begin{bmatrix}A_{P+1}\\B_{P+1}\end{bmatrix}=\begin{bmatrix}a_p\,b_p\\c_p\,d_p\end{bmatrix}\begin{bmatrix}A_p\\B_p\end{bmatrix} \qquad (4.8)$$

Where a_p, b_p, c_p & d_p can be obtained easily which requires multiplication of two 2 × 2 matrix involving Bessel and modified Bessel function. For an initial value of β, using the above 2×2 matrices, one can relate A_N and B_N in term of A_1 and B_1 where the region N is the innermost layer and the region 1 is the outermost region.

$$\begin{bmatrix} A_N \\ B_N \end{bmatrix} = \begin{bmatrix} S_{11} & S_{12} \\ S_{21} & S_{22} \end{bmatrix} \begin{bmatrix} A_1 \\ B_1 \end{bmatrix} \tag{4.9}$$

Where S_{11}, S_{12} etc. are the elements of transfer matrix which is the product of various 2x2 matrices of type discussed above.

4.3 Determination of Propagation Constant

For the guided mode the effective refractive must lie between the maximum and the minimum values of refractive index. Since the field is finite at $r = 0$ and $r = \infty$, the coefficient of B_1 and B_N must satisfy

$$B_1 = 0, \qquad B_N = 0, \tag{4.10}$$

Applying these two conditions, we get from equation (4.10)

$$\begin{bmatrix} A_N \\ 0 \end{bmatrix} = \begin{bmatrix} S_{11} & S_{12} \\ S_{21} & S_{22} \end{bmatrix} \begin{bmatrix} A_1 \\ 0 \end{bmatrix} \tag{4.11}$$

Which implies $S_{21}=0$.

Equation (4.11) is an eigen value equation. Hence in this case by scanning $S_{21}(\beta)$ in the β axis the solution of the above equation will be obtained. Multimode fiber will give us a number of zeros, for the above equation whereas single mode fiber will give only one solution. The solutions in β axis are the mode propagation constants.

4.4 Determination of Leakage Loss

If there is a cladding layer having refractive index higher than or equal to the core index, even the fundamental mode becomes leaky. Calculation of this leakage loss is extremely important for these kinds of fibers. For such leaky modes we have $\beta^2 < k_0^2 n_1^2$, where n_1 is the refractive index of the outermost cladding or the core region. Thus the solution of the outermost cladding is given by the equation (4.4). The equation (4.11) is a complex eigen value equation. $S_{21}(\beta)$ will not be equal to zero now. The propagation constant β now has two parts, the real part (β_r) and the imaginary part (β_i). For leaky mode, the outermost region should correspond to a purely outgoing wave,

we must choose such a linear combination of $J_0(k.r)$ and $Y_0(k.r)$ such that it represents an outgoing wave. For this we choose

$$A_1 = iB_1 \tag{4.12}$$

Thus from the equation (4.9) we have

$$A_N = A_1(S_{11} + iS_{12}) \quad (4.13)$$

$$B_N = A_1(S_{21} + iS_{22}) \quad (4.14)$$

Again we have $\beta^2 < k_0^2 n_N^2$, where n_N is the refractive index of the innermost layer and as before we must have

$$B_N(\beta) = 0 \quad (4.15)$$

This is now a complex eigenvalue equation. We can calculate both the real and imaginary parts of the propagation constant. Now we scan $\left|1/B_N(\beta)\right|^2$ along the real β axis and we obtain Lorentzians, the position of the peak gives the real part of the propagation constant of the mode and the full width at half maxima gives the imaginary part of the mode.

Imaginary part of the propagation constant is the measure of the leakage loss. Loss can be determined by the following relationship:

$$\text{Loss (dB/mm)} = 0.868589 \times 10^4 \times \text{HWHM} \quad (4.16)$$

where the dimension of HWHM is μm^{-1}

Equation was solved and the Lorentzian was obtained by simple numerical technique.

4.5 Basic Principle of Sensing

The basic principle of sensing is to have a mismatch between the diameter of core of uncladded region (sensing region) and core of cladded region. So the whole light from the cladded region does not couple with uncladded region, i.e, some portion of light radiate out when it goes from the cladded region to the sensing region. Hence the modal field is modulated in the sensing region. Hence total power at output is also modulated and become sensitive to the refractive index of the external medium. By measuring the output power and input power we can find out the refractive index of the external medium.

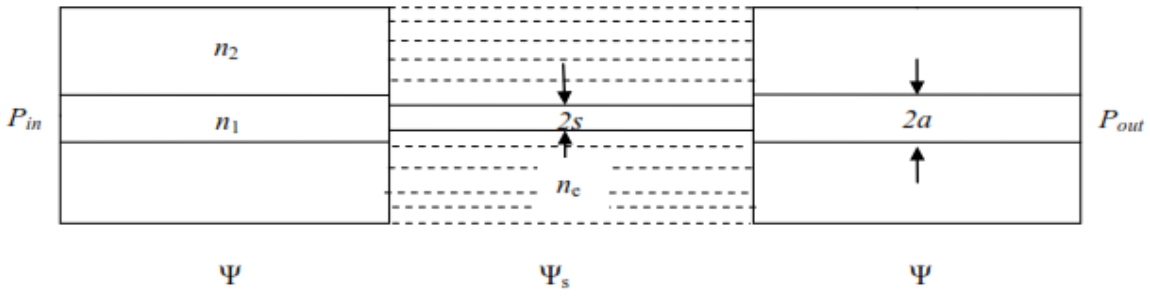

Fig 4.3 Schematic diagram for the core diameter mismatch sensor

Schematic of core diameter mismatch sensor is shown in fig.4.3. n_1, n_2, n_{ex} are refractive indices of

core, cladding and external medium. Here '*a*' and '*s*' defines the core radii in cladded and sensing region respectively. The modal fields in the cldded and the sensing regions are represented by Ψ and Ψ_s respectively. If the sensing region of the fiber is placed into a medium having refractive index different from that of cladding, the modal field distribution changes. The overlap of modal fields in cladded region and sensing region gives estimate of fractional power transfer from the input end to output end. The fractional power transfer is given by

$$\frac{P_{out}}{P_{in}} = T \tag{4.17}$$

where

$$T = \frac{\left|\iint \psi^{*} \psi_s r dr d\phi\right|^2}{\iint |\psi|^2 r dr d\phi \iint |\psi_s|^2 r dr d\phi} \tag{4.18}$$

When n_{ex} = 1 there is strong confinement of modal field in the core of the sensing region and the overlap between ψ and ψ_s is small. As the value of n_{ex} increases the field spreads into the sensing region and the overlap increases. This will change the transmitted optical power.

Chapter 5

Result and Discussion

For the fiber structure proposed in fig. 4.1 and having profile parameter in equ. 4.1, following results are obtained which are responsible for single mode operation and dual shape core fiber based refractive index sensor. The fiber having following parameters:

n_s= 1.444388, n_1= 1.445111, n_2= 1.429871 & a = 15μm. The wavelength of operation used is 1.55µm. Using programming (Appendix A, B & C) and varying the values of d_1 and d_2 calculate losses (dB/m) and select the optimize length of proposed DSC fiber to be under 3 meters. After varying the thickness of sensing region (s) and correspondingly calculating the Transmittance (T) and Maximum resolution , we proposes the best configuration of the said sensor.

To calculate loss to LP_{11} for given DSC fiber for varying d_1 and d_2, plotting graph loss/m vs. d_1 and d_2 and find n_{eff} for first mode LP_{11} for s=15μm:

Table 5.1 Calculation of Loss (dB/m) for LP_{11} mode for d_2=3μm configuration

$d_1(\mu m)$	$d_2(\mu m)$	n_{eff} for LP_{11}	Loss for LP_{11} (dB/km)	Loss for LP_{11} (dB/m)
1	3	1.442412	18612	18.612
2	3	1.444144	11689	11.689
3	3	1.444215	7253	7.253
4	3	1.444267	4461	4.461
5	3	1.444307	2627	2.2627

Table 5.2 Calculation of Loss (dB/m) for LP_{11} mode for d_1=2μm configuration

$d_1(\mu m)$	$d_2(\mu m)$	n_{eff} for LP_{11}	Loss for LP_{11} (dB/km)	Loss for LP_{11} (dB/m)
2	1	1.444163	361818	361.818
2	2	1.444145	61667	61.667
2	3	1.444144	11692	11.692
2	4	1.444144	2261	2.261
2	5	1.444145	439	0.439

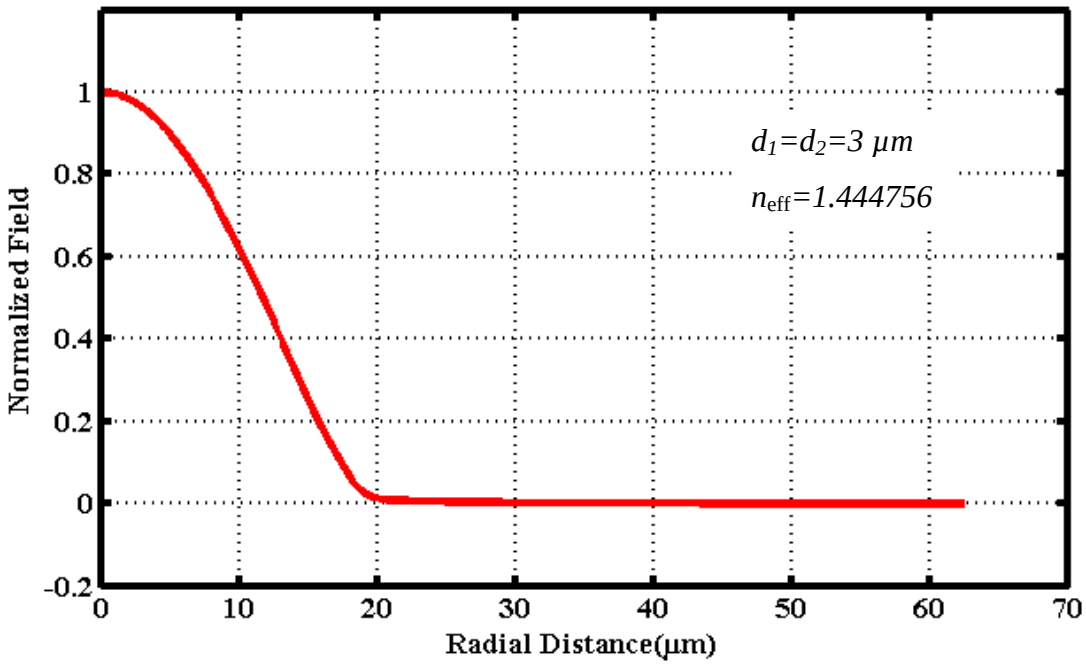

Fig. 5.1 Normalized field vs. radial distance for LP_{01} mode

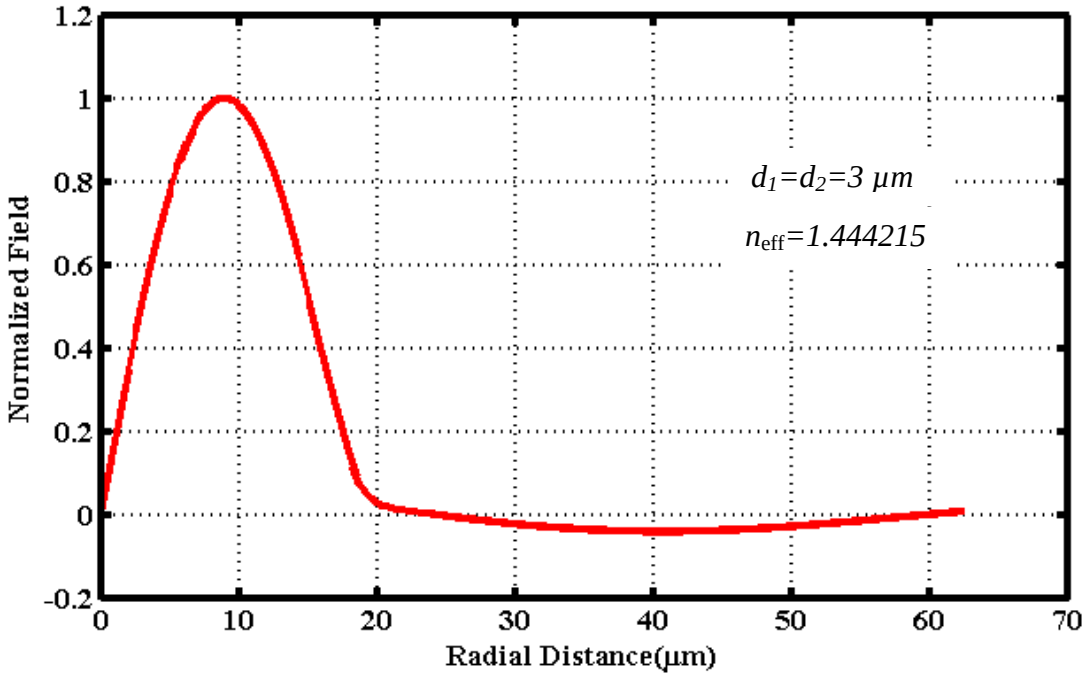

Fig.5.2 Normalized field vs. radial distance for LP_{11} mode

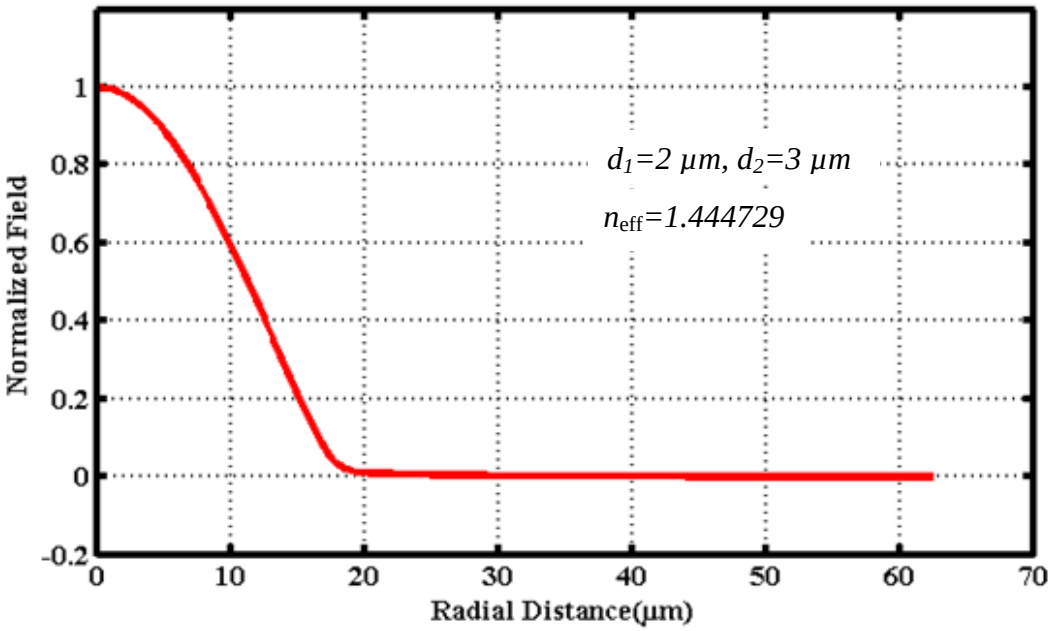

Fig.5.3 Normalized field vs. radial distance for LP_{01} mode

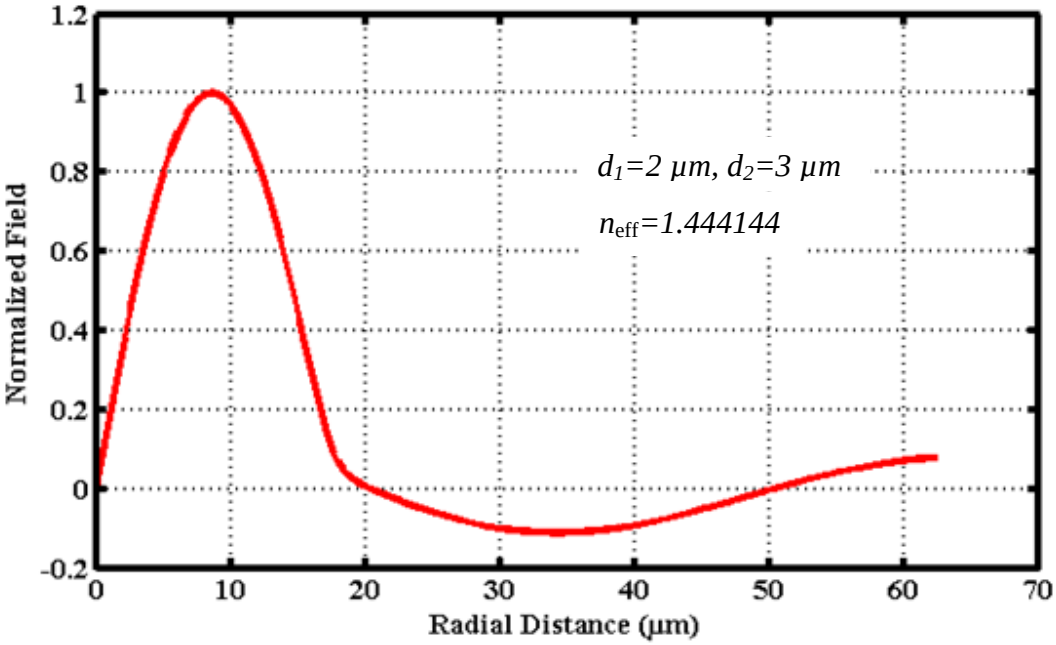

Fig.5.4 Normalized field vs. radial distance for LP_{11}mode

For single mode, the effective length of fiber (L_{SM}) required for leaking out the higher-order modes by introducing a 20dB loss. 20dB rejection ratios is conventionally used for most of the higher-order mode filtering designs as it brings down the power by a factor of SM 100.

By analyzing the above experimental data, we proposed two fiber configurations:

1) d_1=2μm, d_2=3μm (Fiber1) and 2) d_1=d_2= 3μm (Fiber2)

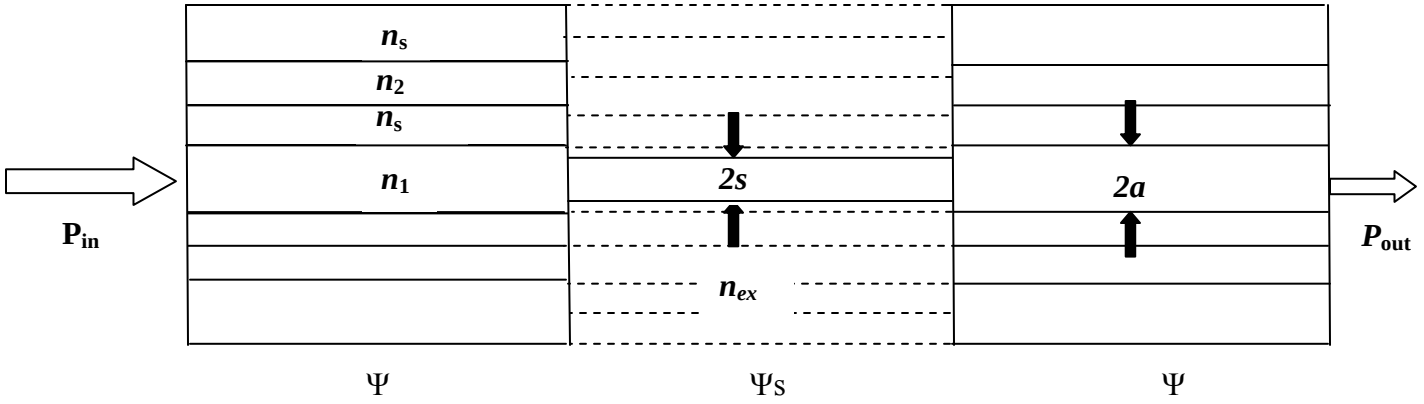

Fig. 5.5 *Schematic diagram of the proposed dual shape core fiber diameter mismatch sensor*

First design & analyze the dual shape core based RI sensor for the fibre1 (d_1=2μm, d_2=3μm) configuration:

5.1 Same Core Diameter for Fiber1 Configuration

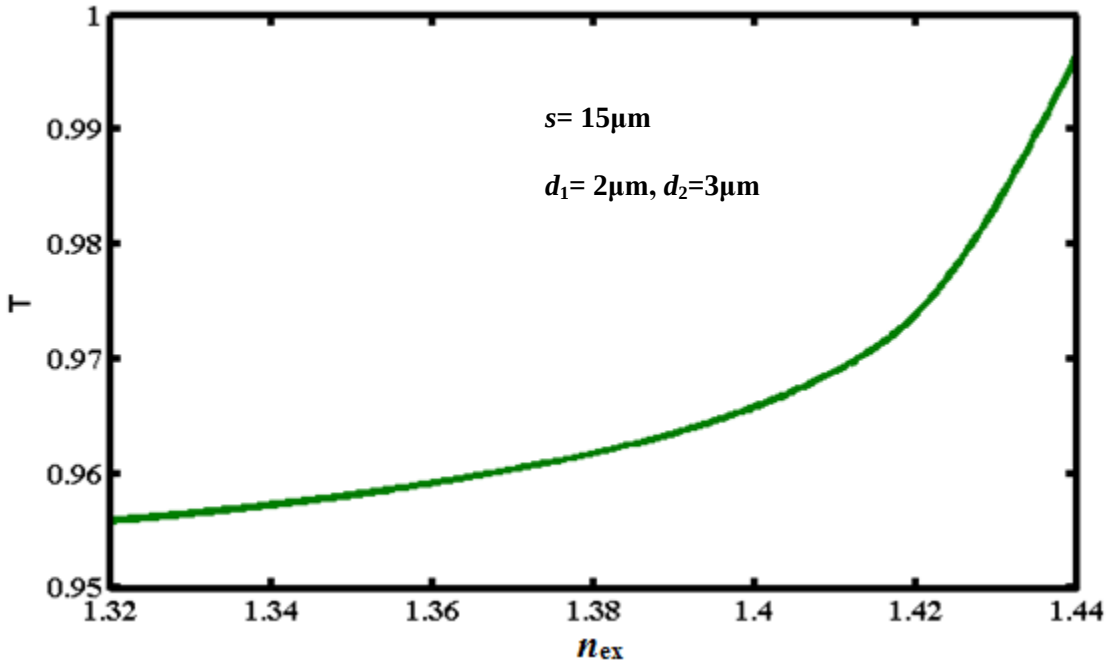

Fig. 5.6 Variation of fractional power transfer with the refractive index of the external medium

The given graph tells that the fractional power transfer (T) varies with different external refractive index (n_{ex}). The total power transfer varies from 95.6% to 99.8% for the variation in external refractive index from 1.32 to 1.44. This shows a small sensitivity for such a large range of refractive index. Hence sensing radius equal to the core radius gives less sensitivity.

The variation of normalized field with radial distance is also shown for in fig.5.7. It can be seen by the figure that the cladded field and field for external refractive index of 1.44 are almost closed to each other. This is due to the mostly power transfer from the cladded region to the sensing region.

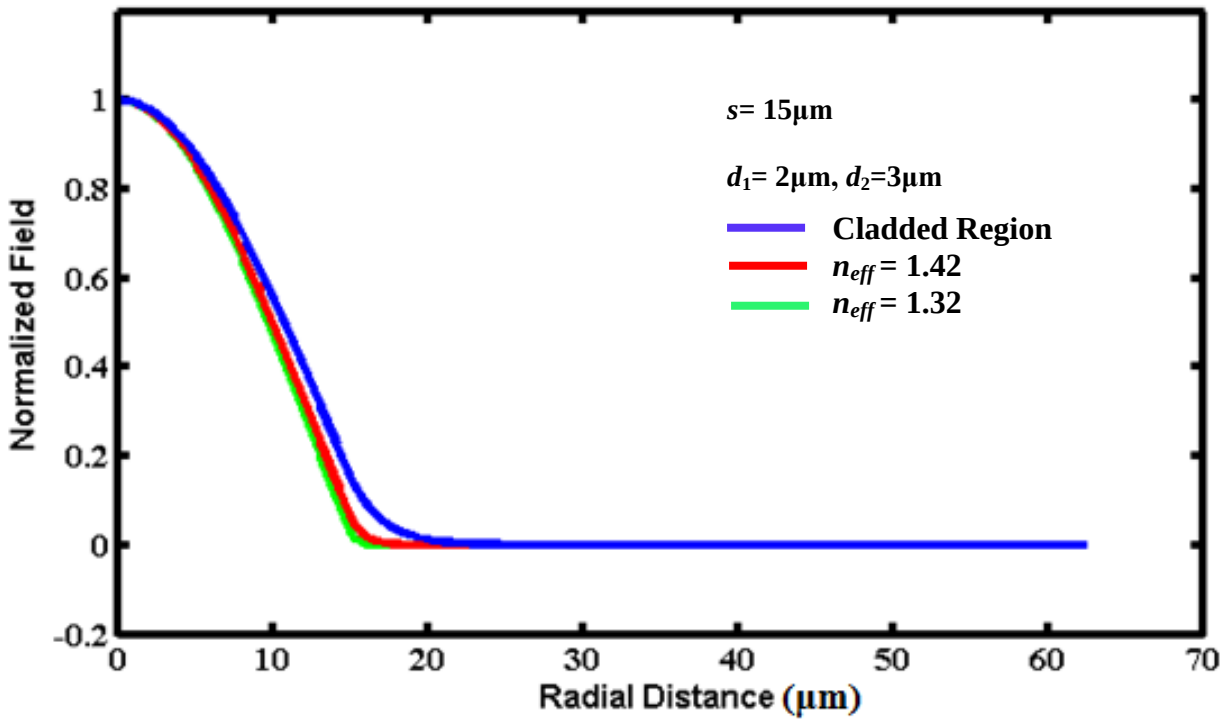

Figure 5.7 Normalized field plot in cladded and sensing region

5.2 Core Diameter Mismatch for Fiber1 Configuration

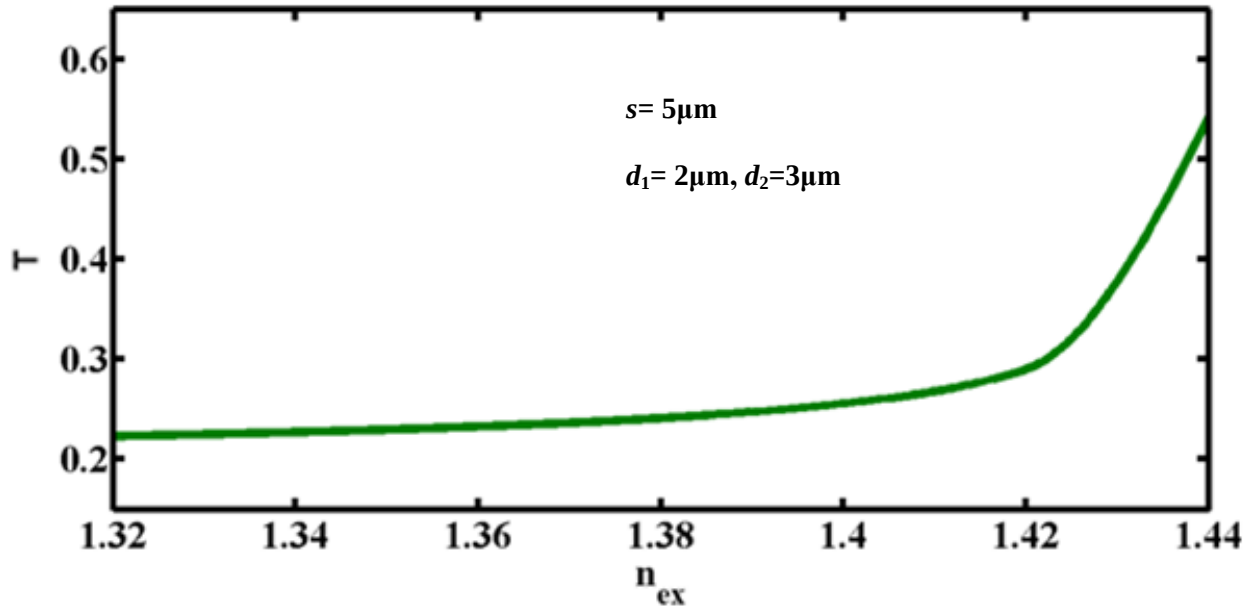

Fig. 5.8 Variation of fractional power transfer with the refractive index of the external medium

Fig. 5.8 shows that the fractional power transfer (T) changes with the change in the Refractive Index of the external medium. As the refractive index of the external medium (n_{ex}) is increased the fractional power transfer is also increased. The T varies from 22% to 54% as the n_{ex} varies from 1.32 to 1.44 for s=5μm. The sensitivity is very high as core diameter mismatch is very high in this case.

Such a large variation in the T is due to the fact that field in the sensing region resembles with the cladded region field on increasing the n_{ex}. The variation of normalized field distribution with radial distance is also shown below. The field penetration in the cladded region is greater than that in the sensing region as the refractive index contrast is greater in the sensing region.

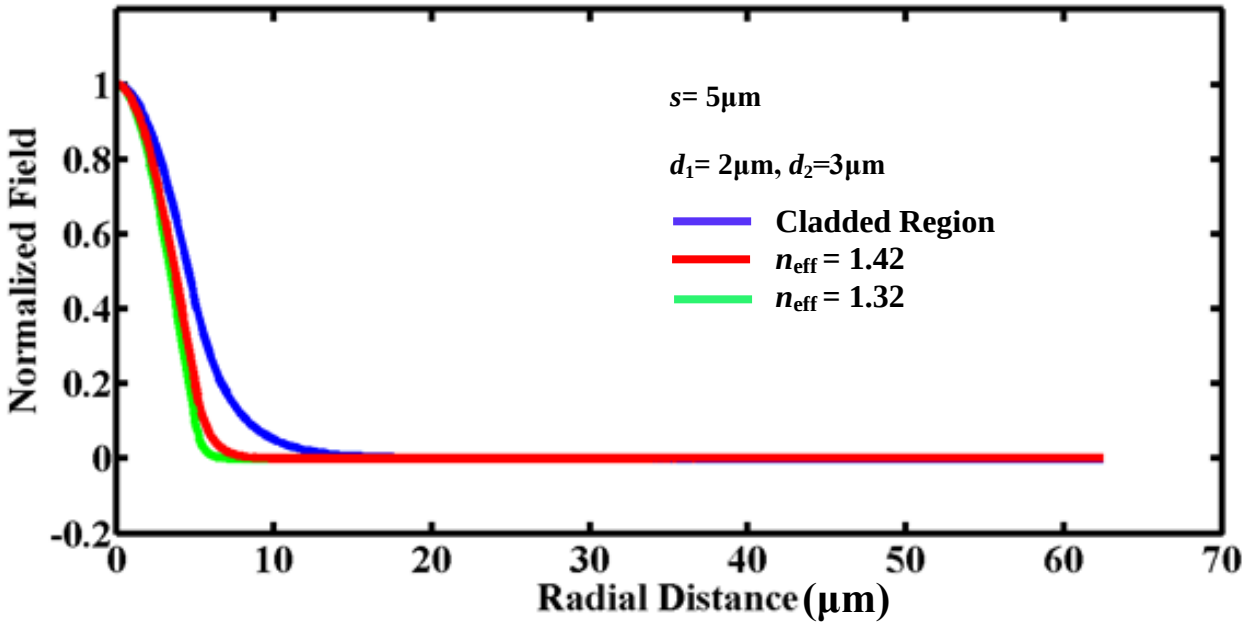

Fig. 5.9 Normalized field plot in cladded and sensing region

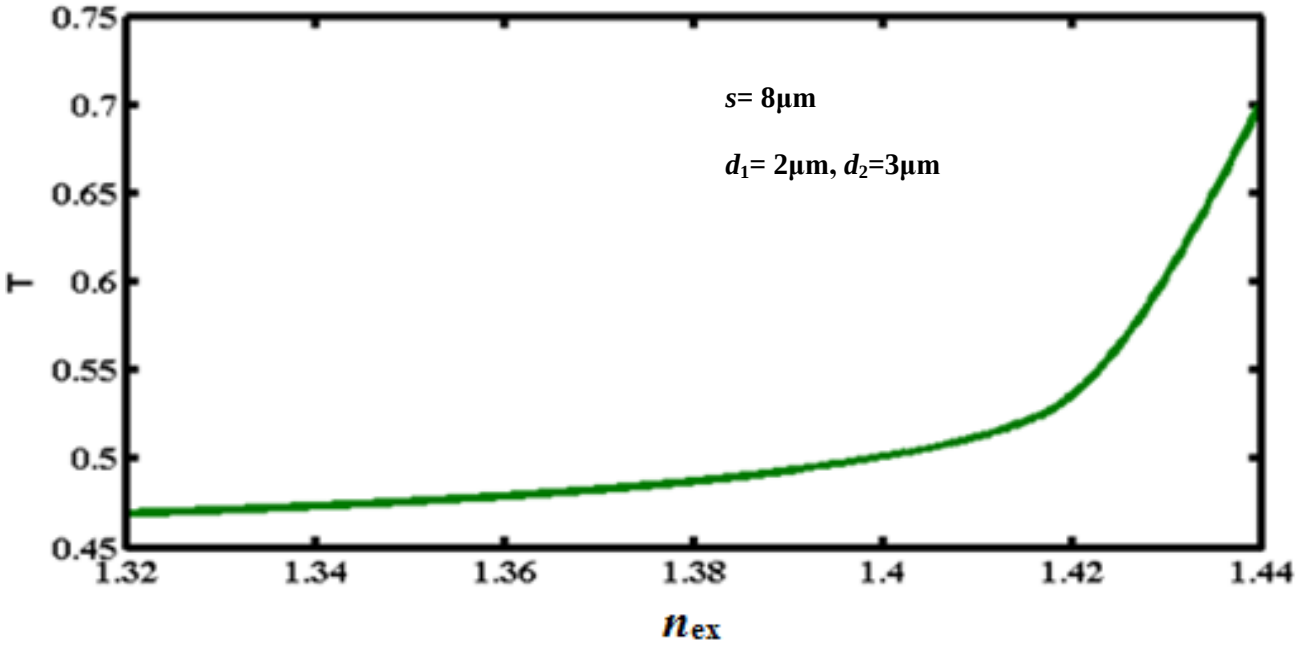

Fig. 5.10 Variation of fractional power transfer with the refractive index of the external medium

The fig.5.10 for s=8μm, gives the variation of fractional power transfer with the external refractive index. The power transfer is from 48% to 70% as refractive index varies from 1.32 to 1.44. In this case the power transfer is more than the s = 5μm case.

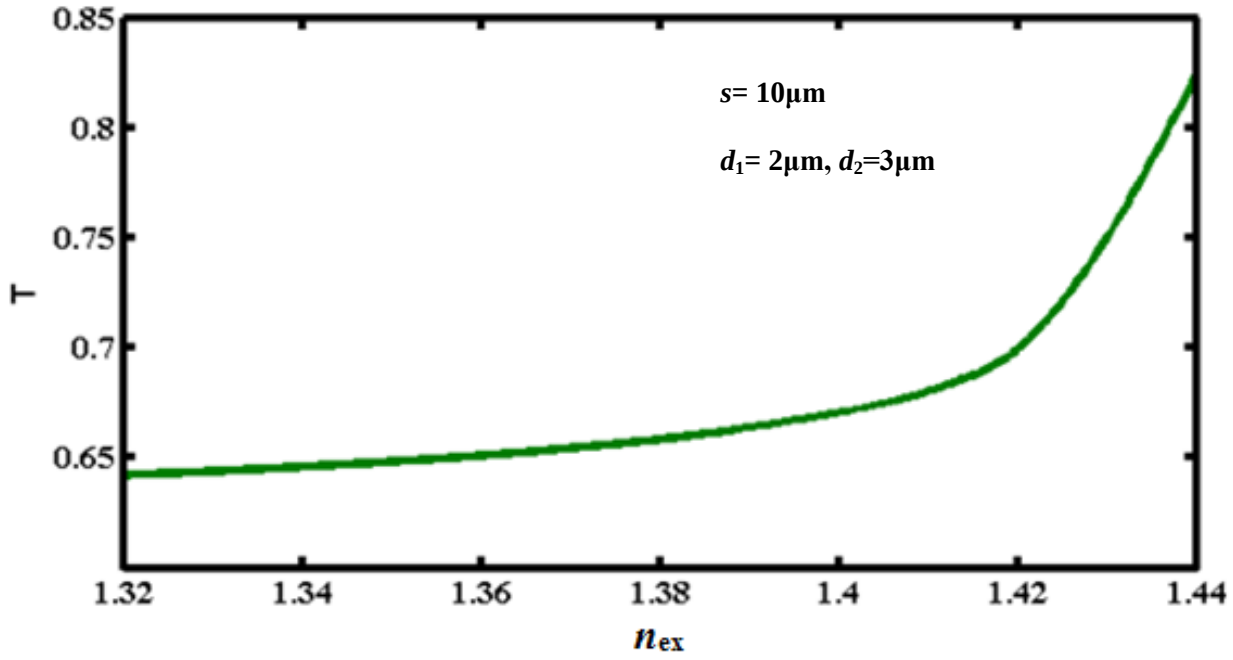

Figure 5.11 Variation of fractional power transfer with the refractive index of the external medium

Fig. 5.11 shows the variation of total power transfer with external refractive index for s=10μm. As the sensing radius is increased the power transfer is also increased. This is due to the fact that large sensing area allows more power to flow into it. The variation of power transfer is from 0.64 to 0.83 for variation in refractive index from 1.32 to 1.44.

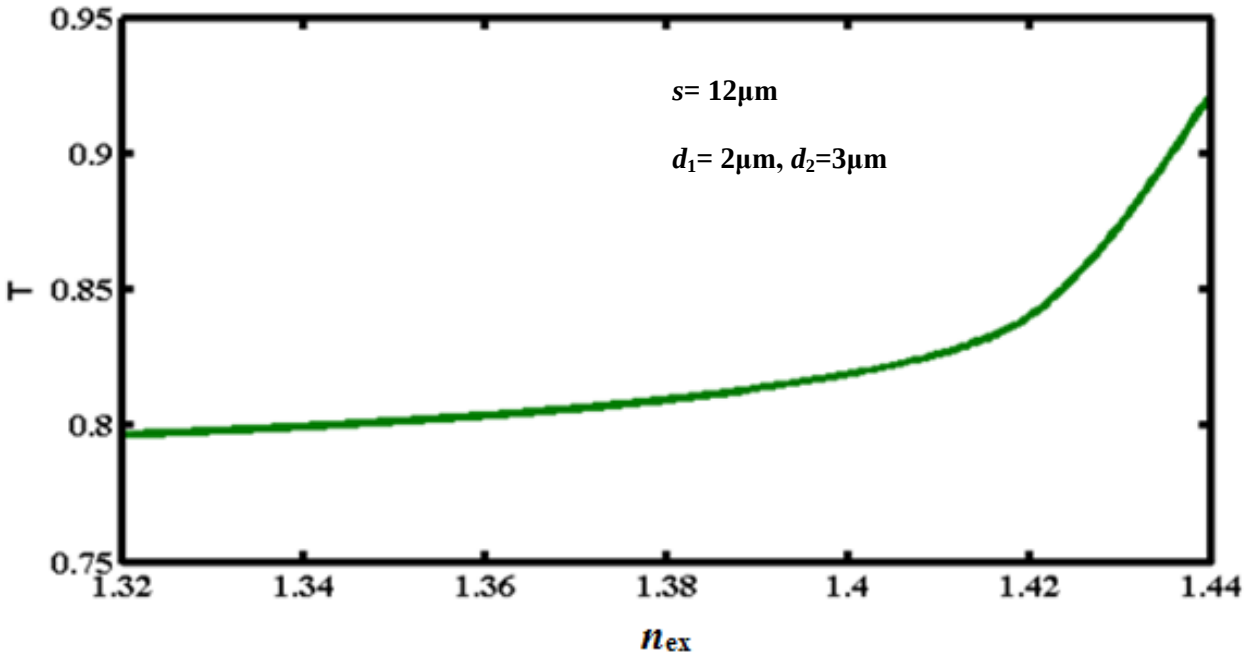

Fig. 5.12 Variation of fractional power transfer with the refractive index of the external medium

The fig.5.12 tells us about the variation of total power transfer with external refractive index for the sensing radius of 12μm. The total power transfer varies from 79% to 92% for the variation of refractive index from 1.32 to 1.44.

The total power transfer for the different sensing radius is plotted on the same graph and shown below.

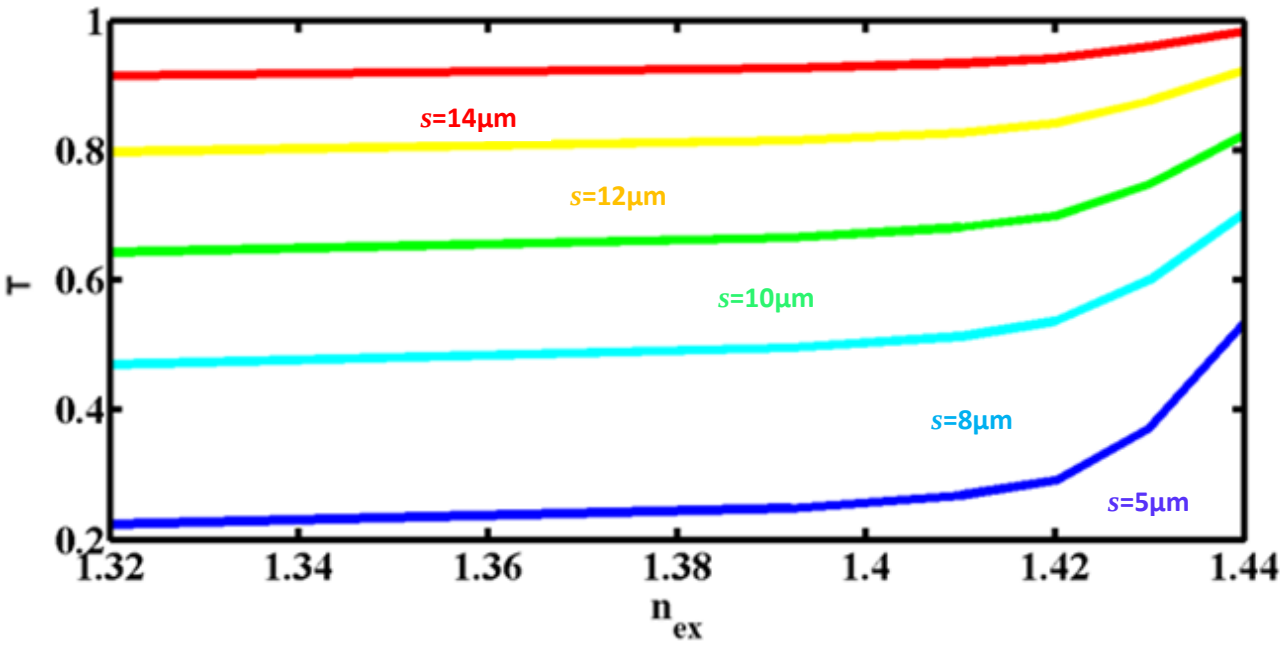

Figure 5.13 Fractional power transfer (*T*) *vs. refractive index of the external medium* (n_{ex}) *for different sensing radius* (*s*) *of fiber*1

We have plotted *T* as a function of n_{ex} for different values of *s*. One can see an improvement in the sensitivity of *T* with n_{ex}. It can also be seen from the above plot that as core diameter mismatch increases the sensitivity increases. *T* varies from approximately 22% to 54% for $s = 5\mu$m when n_{ex} is increased from 1.32 to 1.44. In comparison, in single mode optical fiber refractive index sensor configuration of ref.38 change is from 50% to 78% for $s = 0.7\mu$m. Again in comparison to the multimode-single-mode-multimode configuration of ref.37, change is from 86% to 97%. Hence the above given configuration is far better than given in ref.37 and ref.38. It has good sensitivity for a sensing radius of approximately seven times than the used in ref.37 and ref.38.

.

Now design and analyzed for fibre2 (d_1= d_2=3μm) configuration:

5.3 Same Core Diameter for Fiber2 Configuration

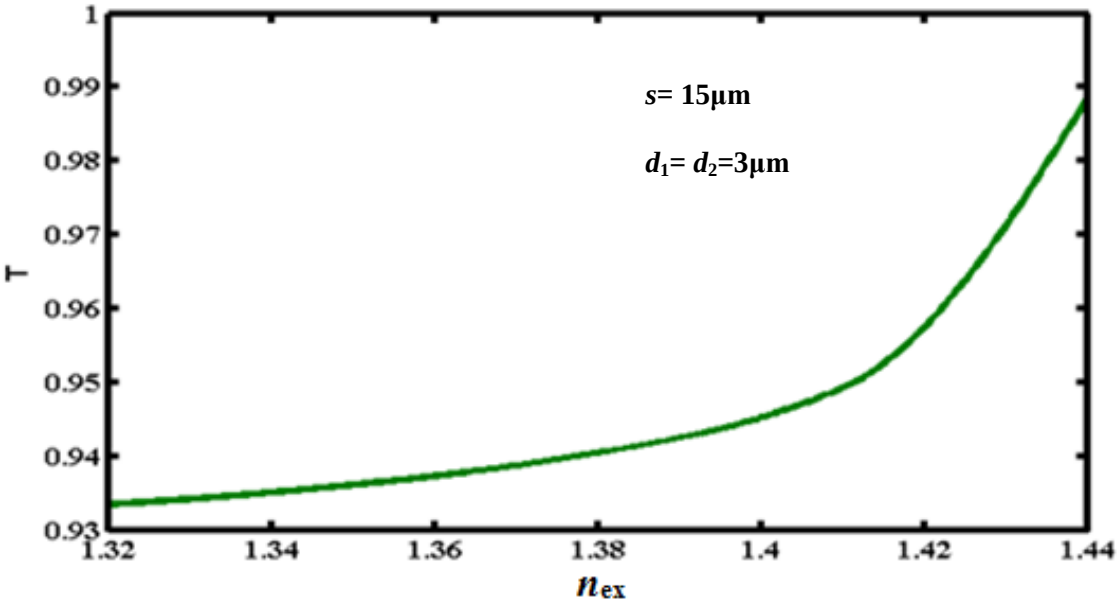

Fig. 5.14 Variation of fractional power transfer with the refractive index of the external medium

The total power transfer varies from 93.6% to 98.9% for the variation in external refractive index from 1.32 to 1.44. This shows a small sensitivity for such a large range of refractive index. Hence sensing radius equal to the core radius gives less sensitivity. The variation of normalized field with radial distance is also shown for in fig.5.15. It can be seen by the figure that the cladded field and field for external refractive index of 1.44 are closed to each other. This is due to the maximum power transfer from the cladded region to the sensing region.

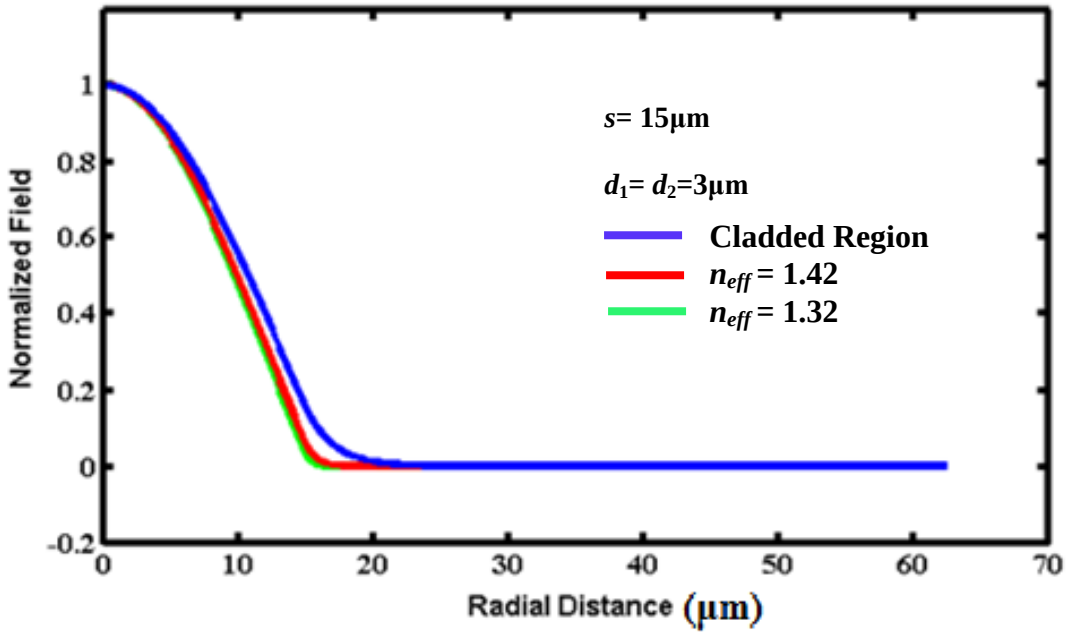

Fig.5.15 Normalized field plot in cladded and sensing region

5.4 Core Diameter Mismatch for Fiber2 Configuration

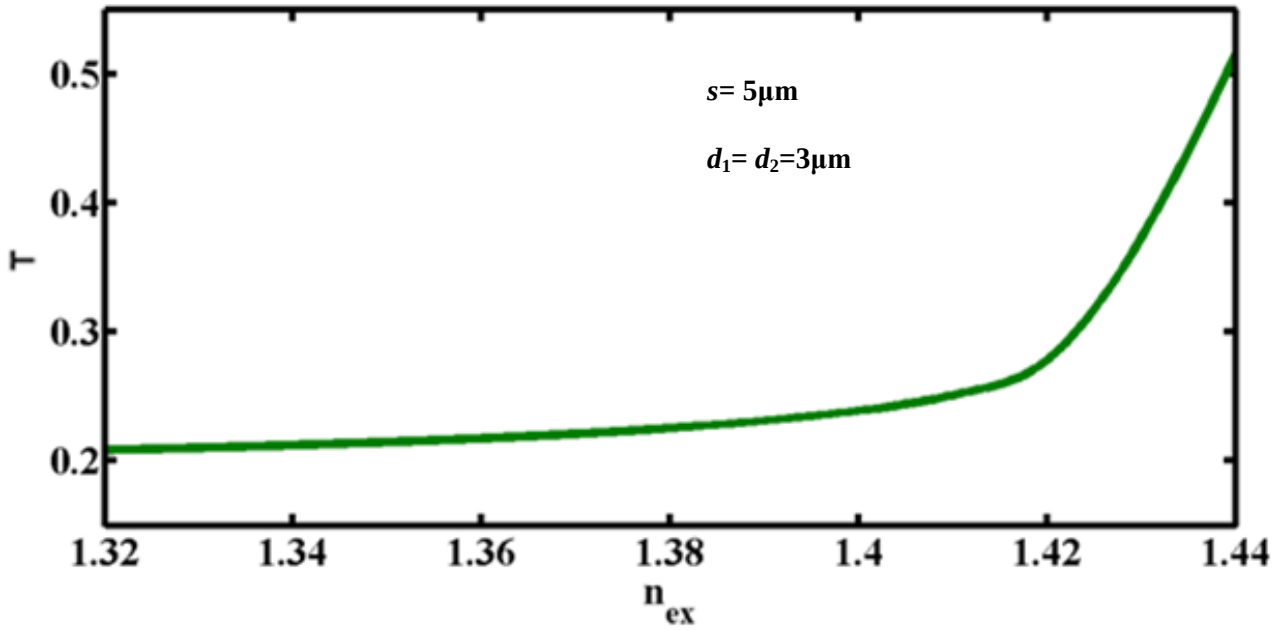

Fig. 5.16 Variation of fractional power transfer with the refractive index of the external medium

Fig. 5.16 shows that the fractional power transfer changes with the change in the refractive index of the external medium. The power transfer from the input to the output varies from 21% to 52% as the refractive index of the external medium varies from 1.32 to 1.44 for *s*=5µm. The variation of normalized field distribution with radial distance is also shown below.

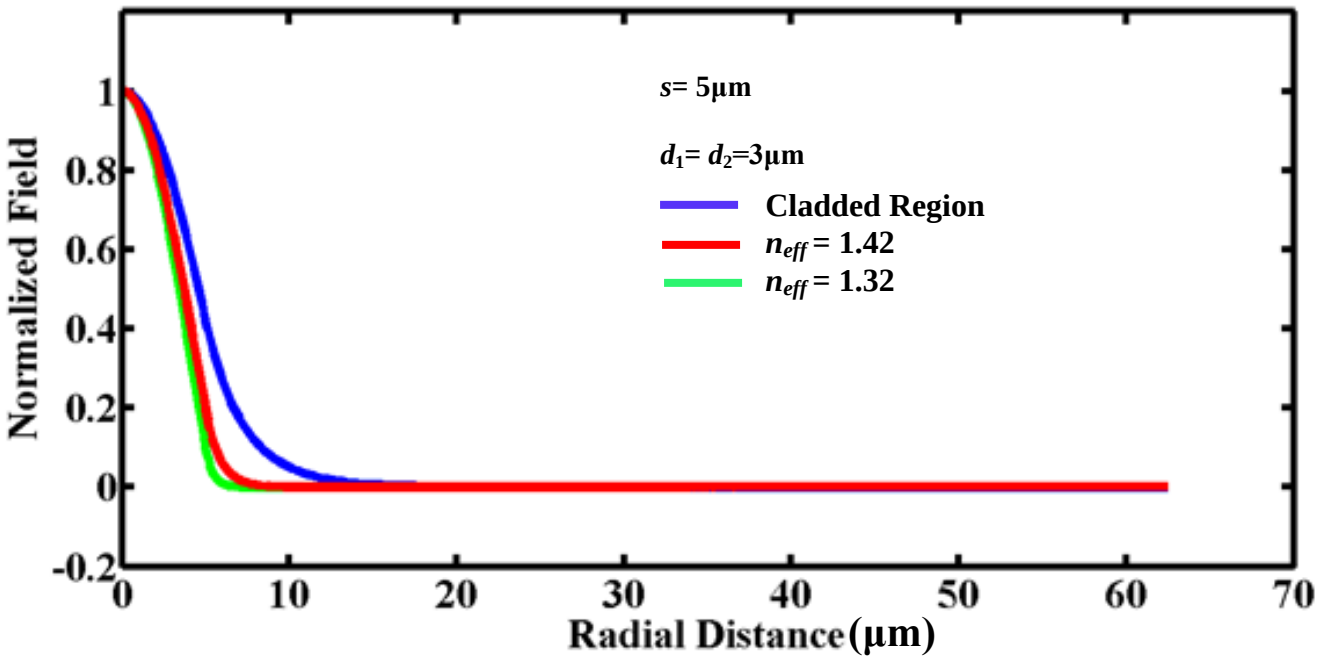

Fig. 5.17 Normalized field plot in cladded and sensing region

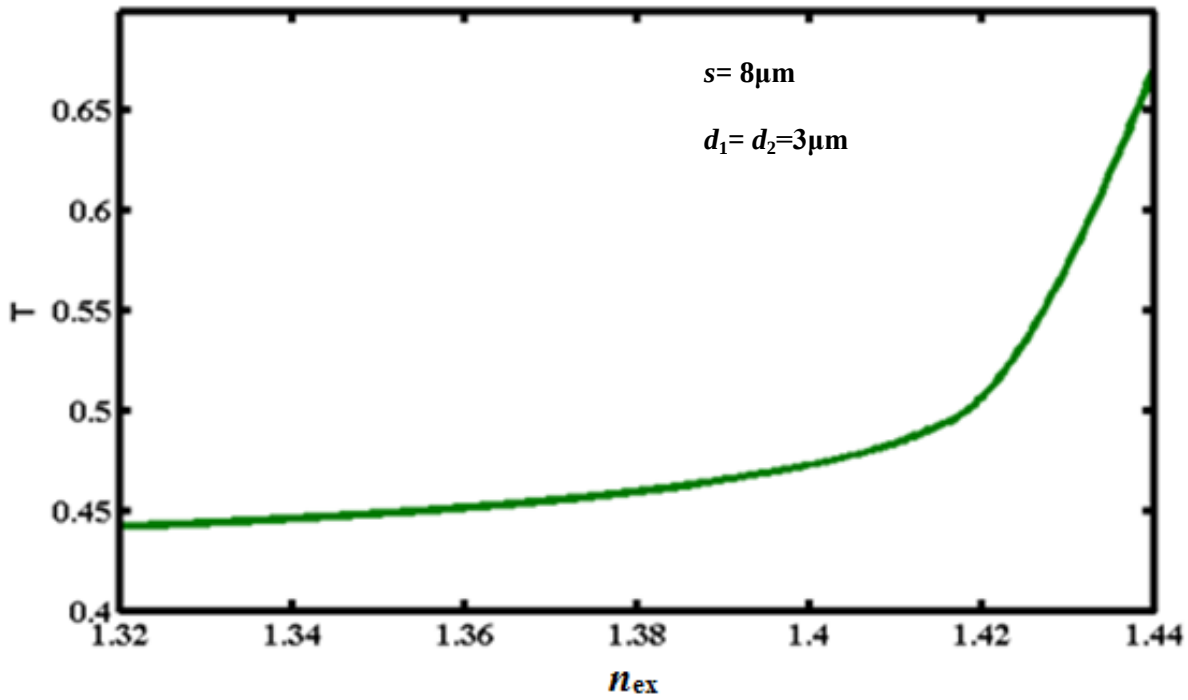

Fig. 5.18 Variation of fractional power transfer with the refractive index of the external medium

The above plot gives the variation of fractional power transfer with the external refractive index for s=8μm. The power transfer is from 44% to 67% as refractive index varies from 1.32 to 1.44. In this case the power transfer is more than the s = 5μm case. As the sensing radius is increased more power can propagate.

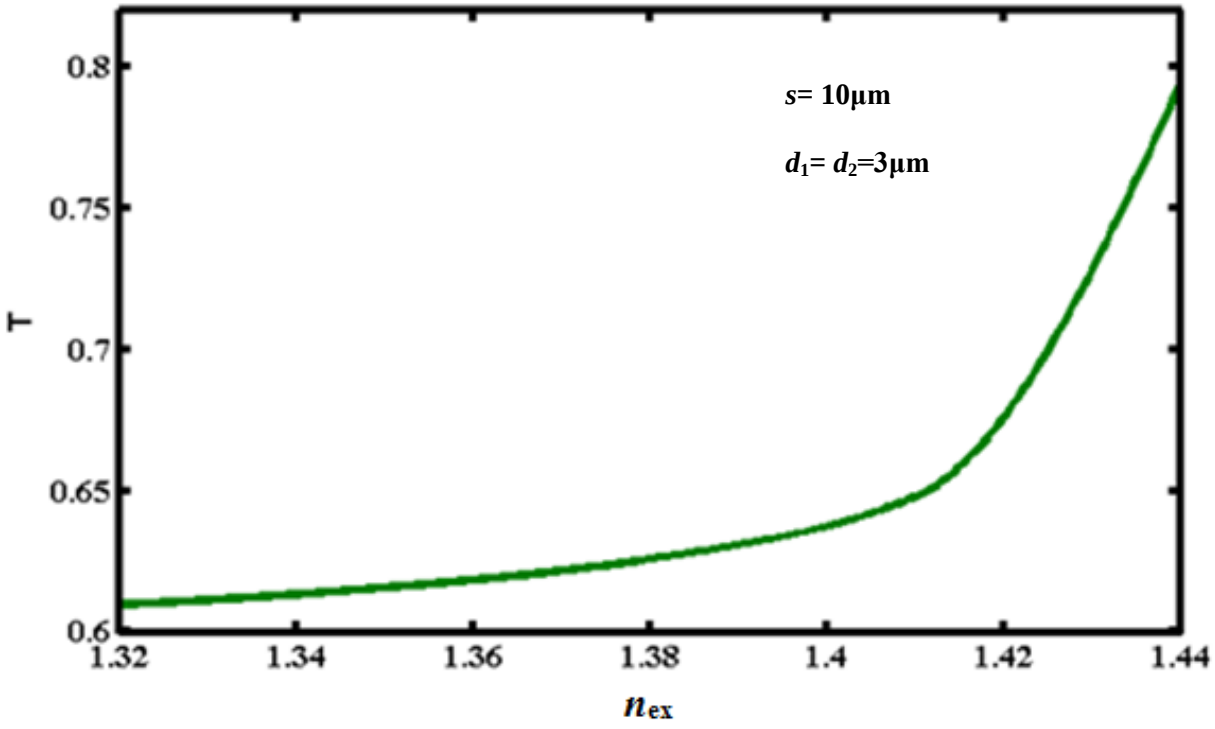

Fig. 5.19 Variation of fractional power transfer with the refractive index of the external medium

Fig. 5.19 shows the variation of total power transfer with external refractive index for s=10μm. The variation of power transfer is from 0.62 to 0.78 for variation in refractive index from 1.32 to 1.44.

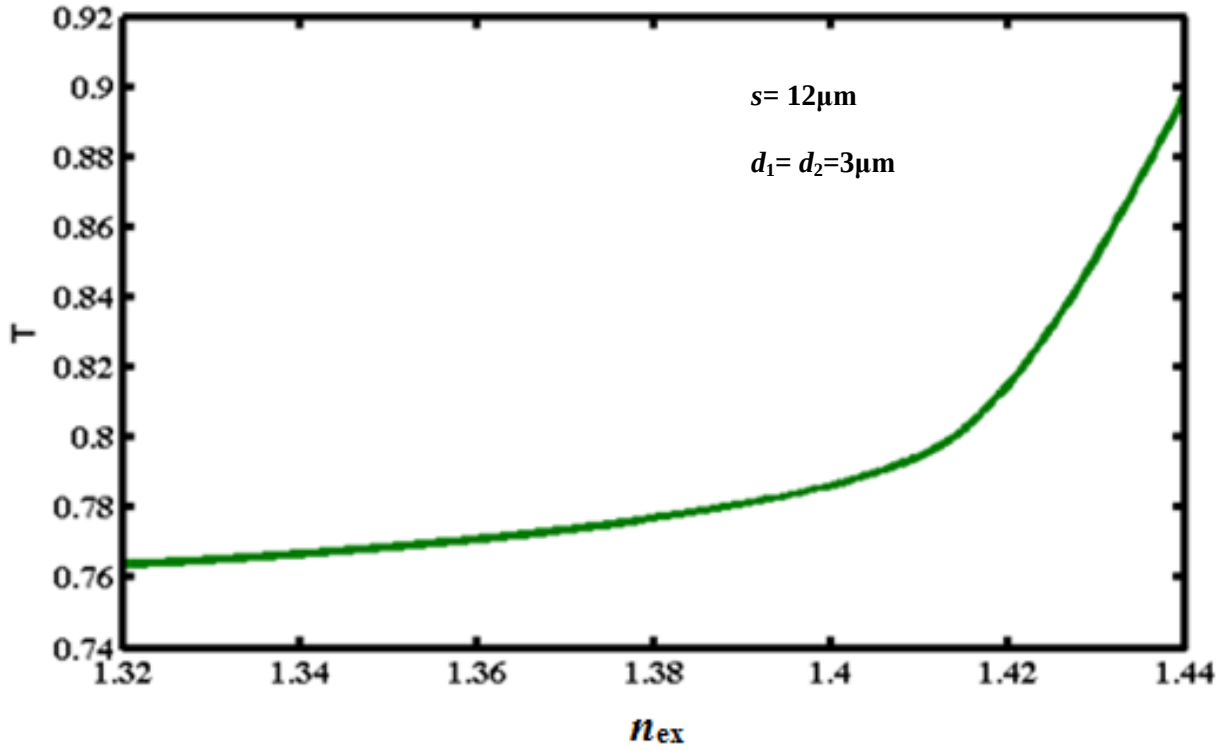

Fig. 5.20 Variation of fractional power transfer with the refractive index of the external medium

Total power transfer with external refractive index for the sensing radius of 12μm varies from 76% to 89% for the variation of refractive index from 1.32 to 1.44. The total power transfer for the different sensing radius is plotted on the same graph and shown below.

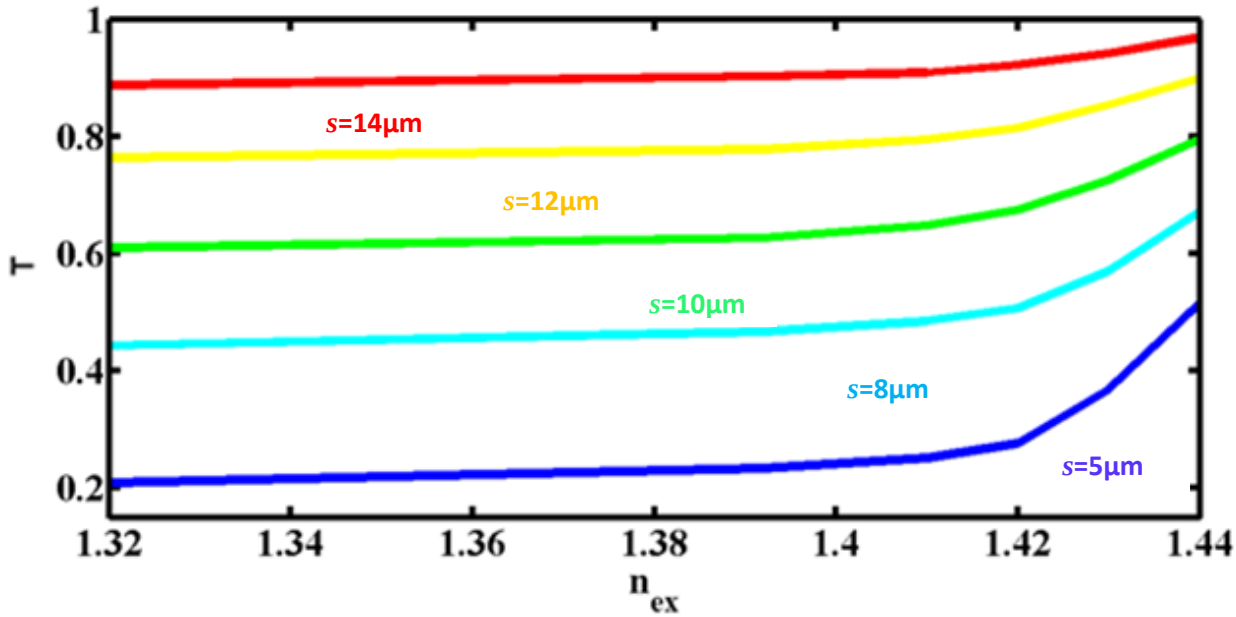

Figure 5.21 Fractional power transfer (T) vs. refractive index of the external medium (n_{ex}) for different sensing radius (s) of fiber2

We have plotted T as a function of n_{ex} for different values of s. One can see an improvement in the sensitivity of T with n_{ex}. It can also be seen from the above plot that as core diameter mismatch increases the sensitivity increases. T varies from approximately 21% to 52% for $s = 5\mu m$ when n_{ex} is increased from 1.32 to 1.44. In comparison, in single mode optical fiber refractive index sensor configuration of ref.38 change is from 50% to 78% for $s = 0.7\mu m$. Again in comparison to the multimode-single-mode-multimode configuration of ref.37, change is from 86% to 97%. Hence the above given configuration is far better than given in ref.37 and ref.38. It has good sensitivity for a sensing radius of approximately seven times than the used in ref.37. We have also calculated the maximum resolution of the proposed sensor. The variation of maximum resolution of designed sensor has also been investigated with sensing radius and shown in fig.5.22 and fig.5.23. For this calculation, we have assumed that T is measured with an accuracy of 1%.

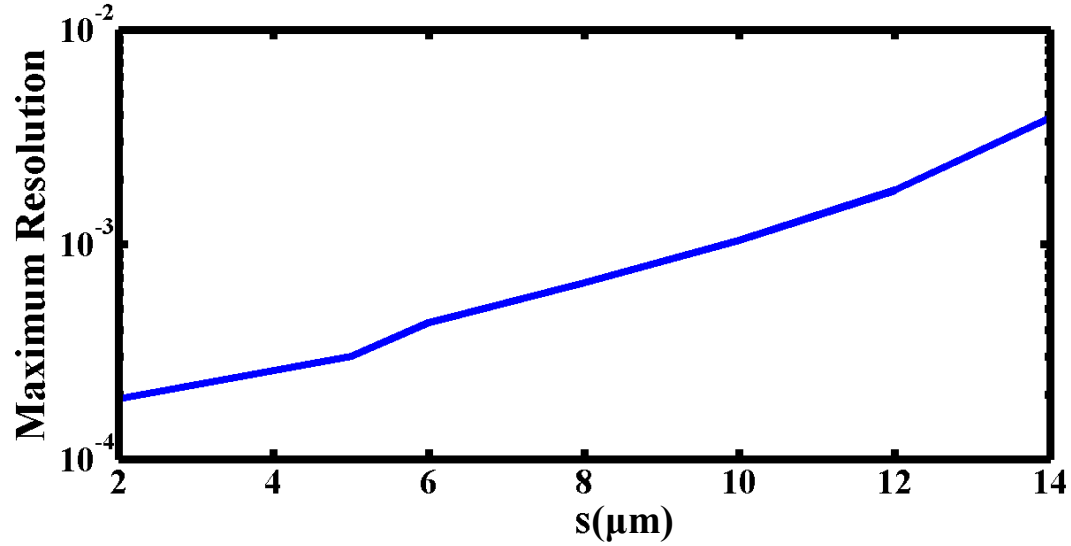

Fig. 5.22 Variation of Maximum resolution with sensing radius of fibre1

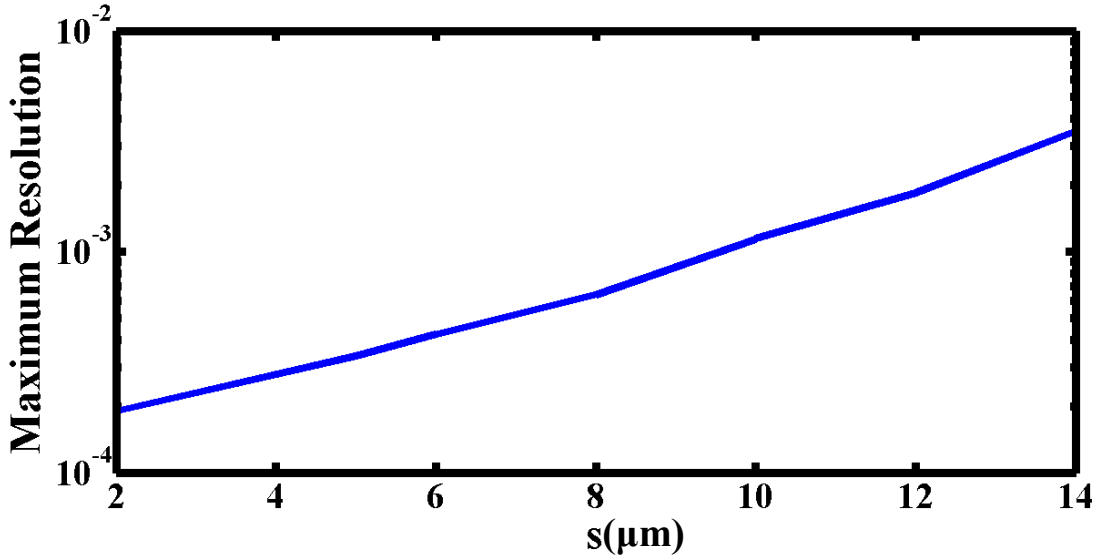

Fig. 5.23 Variation of Maximum resolution with sensing radius of fibre2

Table 5.3 Comparison of Maximum Resolution of Fiber1 and Fiber2

Sensing Radius *s*(μm)	Max. Resolution of Fiber1	Max. Resolution of Fiber2
2	0.00019	0.000189
5	0.00030	0.000337
6	0.00043	0.000420
8	0.00066	0.000638
10	0.00104	0.001140
12	0.00178	0.001838
14	0.00386	0.003500

The above table and graphs shows that maximum resolution of the sensor varies with sensing radius. Due to increase in modal field mismatch, sensitivity of the sensor increases with the decrease in the sensing radius or increase in core diameter mismatch. Sensing resolution decreases from 1.9×10^{-4} to 3.86×10^{-3} when sensing radius increases from 2 to 14μm for fibre1 around n_{ex}=1.44, similarly sensing resolution decreases from 1.89×10^{-4} to 3.5×10^{-3} when sensing radius increases from 2 to 14μm for fibre2 around n_{ex}=1.44. For the sensing radius of 2μm the maximum resolution is of order of 10^{-4}, however, at this size it makes the devices very difficult for practical applications. We have used the smallest sensing radius of 5μm with a maximum resolution of 3×10^{-4} of fibre1 and 3.37×10^{-4} of fibre2, which is almost 3 times better than ref.38 even with 7 times larger sensing core radius.

Chapter 6

Conclusion and Scope for Future Work

6.1 Conclusion and Scope for future work

A dual shape core (DSC) fiber based refractive index sensor is proposed with a single fiber having effective single mode operation. Single-mode operation is made possible with the help of certain design parameters due to which higher order modes are leaked out. Due to DSC & large core area it can support large power and is also less fragile. This is a great advantage. Apart from this, T varies from approximately 22% to 54% for s = 5μm & d_1=2μm, d_2=3μm (fiber1) and 21% to 52% for s = 5μm & d_1=d_2=3μm (fiber2) when n is increased from 1.32 to 1.44. In comparison, in single mode optical fiber refractive index sensor configuration of ref.38 change is from 50% to 78% for s = 0.7 μm. Again in comparison to the multimode-single-mode-multimode configuration of ref.37, change is from 86% to 97%. The resolution is also estimated for the proposed sensor and found its maximum value to be 1.89×10^{-4} around n_{ex}= 1.44. In comparison, in single mode optical fiber refractive index sensor configuration of ref.38 maximum resolution is 9×10^{-4} around n = 1.44. Transmittance of the fibre1 configuration is more than the fibre2 configuration for given n_{ex}, because the fundamental mode is well confined in former configuration as shown comparatively in fig.5.3 & fig.5.1 respectively. The results indicate that the core diameter mismatch sensor, in which a part of the core has also been removed, is more sensitive to the same core diameter sensor. Also as we increase the core diameter mismatch the sensitivity also increases. This is due to fact that in core diameter mismatches the overlapping of modal fields between the input region and the sensing region is less due to modal field mismatch which takes place due to both core diameter mismatch and refractive index mismatch. So, the variation of the output power is greater for the case of core diameter mismatch. Hence, the coupling of light between the cladded and sensing region is less for it. Sensitivity increases when the coupling of light between two regions decreases, so the sensitivity is greater for the case of core diameter mismatch.

The proposed sensor can be used as a compact ***Refractometer***. It can also be used for other wavelengths for which sensitivity may be enhanced. The fiber parameter can be tuned to design the sensor for different band of operating wavelength.

References

1. A. Ghatak and K. Thyagrajan, “Introduction to fiber optics”
2. J.M. Senior, “Optical fiber Communication”
3. G. P. Agarwal, “Fiber-optic communication system”
4. G. Keiser , “*Optical Fiber Communications”*
5. K. Thyagrajan; A.K. Ghatak (10 September 2007), “Fiber Optic Essentials”, Wiley-Interscience. pp. 34–. ISBN 978-0-470-09742-7. Retrieved 1 May 2012.
6. A Mosheky, Zaid; Melling, J. Peter ; Thomson, Mary A. (June 2001). "In situ real-time monitoring of a fermentation reaction using a fiber-optic FT-IR probe" (PDF). Spectroscopy
7. Melling, Peter; Thomson, Mary (October 2002). "Reaction monitoring in small reactors and tight spaces" (PDF). American Laboratory News.
8. Melling, J. Peter ; Thomson, Mary (2002), "Fiber-optic probes for mid-infrared spectrometry" (PDF). In Chalmers, M. John; Griffiths, R. Peter (eds.). Handbook of vibrational spectroscopy wiley.
9. P. St. J. Russell, “Photonic crystal fibers”, Science, vol.299, pp. 358-360 (2003).
10. W. Liang, Y. Huang, Y. Xu, R. K. Lee, and A. Yariv, “Highly sensitive fiber bragg grating refractive index sensors”, Appl. Phys. Lett, vol.86, pp. 122-126 (2005).
11. Tbps over a Single Optical Fiber: Successful Demonstration of World's Largest Capacity – 145 digital high-definition movies transmitted in one second. NTT Press Release. September 29, 2006.
12. M. S. Alfiad, et al. (2008). "111 Gb/s Polmux-RZ-DQPSK Transmission over 1140 km of SSMF with 10.7 Gb/s NRZ-OOK Neighbours".Proceedings Ecoc 2008.pp. Mo.4.E.2.
13. S. Yao, “Polarization in Fiber Systems: Squeezing out more bandwidth”, The Photonics Handbook, Laurin Publishing, 2003, p. 1.
14. Ciena, JANET Delivers Europe’s First 40 Gbps Wavelength Service 07/09/2007. Retrieved 29 Oct 2009.
15. "Ultrafast fibre optics set new speed record". New Scientist. 2011-04-29. Retrieved 2012-02-26.
16. "NEC and Corning achieve petabit optical transmission". Optics.org. 2013-01-22. Retrieved 2013-01-23.
17. Bell Labs breaks optical transmission record, 100 Petabit per second kilometer barrier. Physorg. September 29, 2009.

18. Siemen's claim to a fiber optic line that can not be tapped. Retrieved 18 Dec 2009.
19. V. Rastogi and K. S. Chiang, “Propagation characteristics of a segmented cladding fiber”, Opt. Lett., vol.26, pp.491-496 (2001).
20. M. E. Fermann, “Single-mode excitation of multimode fibers with ultra-short pulses”, Opt. Lett. 23 (1), 52 (1998).
21. H. L. Offerhaus et al., “High-energy single-transverse-mode Q-switched fiber laser based on a multimode large-mode-area erbium-doped fiber”, Opt. Lett. 23 (21), 1683 (1998).
22. J. P. Koplow et al., “Single-mode operation of a coiled multimode fiber amplifier”, Opt. Lett. 25 (7), 442 (2000).
23. S. Wielandy, “Implications of higher-order mode content in large mode area fibers with good beam quality”, Opt. Express 15 (23), 15402 (2007).
24. Y. Shizhuo, K. W. Chung, H. Liu, P. Kurtz and K. Reichard, “A new design for nonzero dispersion shifted fiber with a large effective area over 100 μm and low bending and splicing loss”, Opt. Comm., vol.177, pp.225-229 (2000).
25. S. Sandgren, H. Ahlfeldt, B. Sahlgren, R. Stubbe, and G. Edwall, “Fiber optical Bragg grating refractometer”, Fiber Integr. Opt., vol.17, pp. 51–62 (1998).
26. L. G. Cohen, D. Marcus and W. L. Mammuel, “Radiating leaky mode losses in single mode light guide and depressed index claddings”, IEEE trans. J. Quant. Electron., vol.18, pp. 1467-1471 (1982).
27. Thesis (PH.D.)—University of Waterloo (Canada), 1991. Source: “Dissertation Abstracts International”, Volume: 53-11, Section: B, page: 5786.
28. D. B. Stegall and T. Erdogan, “Leaky cladding mode propagation in long period fiber grating devices” IEEE Photon Technol. Lett. vol.11, pp. 343-345 (1999).
29. X. Shu, L. Zhang and I. Bennion, “Sensitivity characteristics of long period fiber gratings”, J Lightwave Technology, vol.20, pp. 255-266 (1999).
30. V. Rastogi and K.S. Chiang, “Long period gratings in planar optical waveguides”, Appl. Opt. vol.41, pp. 6351-6355 (2002).
31. D. Monzoon, V. Joel, D. Talavera and D. Luna, “Optical surface Plasmon response sensor with multiple resonance peaks”, Appl. Opt. vol.43, pp. 765-770 (2004).
32. R. M. Beiu, C.D. Stanescu and V. Beiu , “Unique In-Fiber Photonic Crystal Sensor”.

33. A. Iadicicco, S. Campopiano, A. Cutolo, M. Giordano, and A. Cusano, , "Nonuniform Thinned Fiber Bragg Gratings for Simultaneous refractive Indexand Temperature Measurements", IEEE Photonics Technology Letters, vol. 17, No. 7, July 2005.
34. J. Villatoro, D. Monzo´ N. Herna´ndez and D. Talavera, "High resolution refractive index sensing with cladded multimode tapered optical fibre", electronics letters 22nd January 2004 vol. 40 No.2.
35. D. Chen, G. Hu, and L. Chen, "Dual-Core Photonic Crystal Fiber for Hydrostatic Pressure Sensing", vol. 23, No. 24, December 15, 2011.
36. W. Yuan, G. E. Town, and O. Bang "Refractive Index Sensing in an All-Solid Twin-Core Photonic Bandgap Fiber", IEEE Sensors Journal, vol. 10, No. 7, July 2010.
37. J. Villatoro and D. Monzoon, "Low-cost optical fiber refractive-index sensor based on core diameter mismatch", J. LightwaveTechnol, vol.24, pp. 1409-1411 (2006).
38. K. Kamakshi, V. Rastogi, A. Kumar and J. Rai, "Design and Fabrication of a Single-Mode Optical Fiber Based Refractive-Index Sensor", vol. 52, No. 6, pp. 1408-1410, June 2010.
39. D. Monzoon, J. Villatoro and D. Luna, "Miniature optical refractrometer using cladded multimode tapered tips", Sens Actuator B Chem. vol.110, pp.36-40 (2005).
40. A. Kumar and V. Rastogi, "Design and Analysis of Dual-Shape-Core Large Mode Area Fiber", vol. 50, No. 25, 1 September 2011.

Appendix A

```
%This program is to find the fractional power transfer for different n_ex

Clear all
Format long;
n_core=1.445110;
nmode=1;
s=15;          % sensing radius
c=62.5;        % total radial region
l=0;
L=1.55;        % Wavelength in micron
r=linspace(0,c,501);
Tf=[];
      n=[];step=1
for nex=1.3200e+000:2.0*10^(-2):1.44e+000;
nex
      [V,neff_med] = bisec(n_core,nex,s,l,L);
         T2 =diametermismatch_Tl(n_core,nex,neff_med,nmode,s,c,r,l,L)
         n=[n,nex];
Tf=[Tf,T2];
%          modalfield(n_core,nex,neff_med,nmode,s,c,r,l,L)
step=step+1
end
figure
plot(n,Tf,'linewidth',3)
xlabel('n_e_x','FontSize',12,'FontWeight','bold');
ylabel ('T','FontSize',12,'FontWeight','bold');
legend ('s=15?m','FontSize',10,'FontWeight','bold');
```

Appendix B

```
%functional program to draw modal field for core diameter mismatch
% function [d11] = modalfield(n_core,nex,neff_med,s,c,l,L)

% n_core=1.445110; nex=1.32 to 1.44;
% neff_med=[1.449078395049764  1.445243130064973]; s=10; c=62.5; l=0; L=1.55;
function [fd] = modalfield(n_core,nex,neff_med,nmode,s,c,r,l,L);
formatlong;
phi=0;
        k0=2*pi/L;
        j=1;
        d11=[];
beta_med=neff_med(nmode).*k0;
u_med(nmode)=s.*sqrt((k0*n_core)^2-beta_med.^2);
w_med(nmode)=s.*sqrt(beta_med.^2-(k0*nex)^2);

while j<=length(r)
if  r(j)<s;

psi_med=(1./besselj(l,u_med(nmode))).*besselj(l,u_med(nmode).*r(j)/s).*(cos(l*phi));
else r(j)>s & r(j)<=c;

psi_med=(1./besselk(l,w_med(nmode))).*besselk(l,w_med(nmode).*r(j)/s).*(cos(l*phi));
end
             d11=[d11 psi_med];
              j=j+1;
end
if d11(:,1)<0
          d11=-d11;
end
dnorm=d11/max(d11)
fd=[r' dnorm'];
end
```

Appendix C

```
function [fpt] = diametermismatch_Tl(n_core,nex,neff_med,nmode,s,c,r,l,L)
fd = modalfield(n_core,nex,neff_med,nmode,s,c,r,l,L);
      d11=fd(:,2);   % sensing region
% Generate d1 from load file
Load 'field.dat'
     d1=field(:,2);
     R=field(:,1);
T_num=trapz(R,((d11.*d1).*R));
     A=sqrt(trapz(R,((d11.*d11).*R)));
     B=sqrt(trapz(R,((d1.*d1).*R)));
     T=abs((T_num)/(A.*B));
fpt=T.^2;
%       hold on
     plot(fd(:,1),fd(:,2),'linewidth',3)
xlabel ('Radial Distance','FontSize',12,'FontWeight','bold');
ylabel ('Normalized Field','FontSize',12,'FontWeight','bold');
hold on
plot(R,d11)
end
```